Department of Biomaterials, Institute of Clinical Sciences,
Sahlgrenska Academy at University of Gothenburg, Göteborg,
Sweden

On a novel technique for preparation and analysis of the implant surface and its interface to bone

by

Anders Palmquist

UNIVERSITY OF GOTHENBURG
2008

Department of Biomaterials
Institute of Clinical Sciences
Sahlgrenska Academy
University of Gothenburg

Correspondence:
Anders Palmquist
Department of Biomaterials
Box 412
SE-405 30 Göteborg
Sweden

E-mail: anders.palmquist@biomaterials.gu.se

ISBN: 978-91-628-7504-6

Printed in Sweden
Geson Hylte Tryck

Printed in 300 copies

Abstract

The ultrastructural and biomechanical properties of the bone-implant interface are important factors for implant performance. For further understanding of the osseointegration process novel tools enabling analysis of the intact interface in high resolution is needed, preferably combined with histology and biomechanical tests. Initial studies using focused ion beam microscopy (FIB) for TEM sample preparation have shown promising results.

The general aim of the thesis was to evaluate FIB for TEM sample preparation using different lift-out techniques and protection modes applied on the implant surface and its interface to bone tissue. Further, another aim was to combine different surface analytical and biological evaluation techniques with FIB/TEM in order to correlate the ultrastructure and the biomechanics of the interface using a new implant surface with micro- and nano-scale surface features.

A combination of different techniques was used for surface analysis of commercially available and test implants made of commercially pure titanium (Ti) and titanium alloy (Ti6Al4V). Scanning electron microscopy (SEM) and interference microscopy were used for surface topographical analyses. Auger electron spectroscopy (AES) was used for surface chemical analysis and depth profiling. Morphological and structural analysis was performed using FIB/TEM. An amputation prosthesis which was retrieved after 11 years in clinical function was analyzed by histology, histomorphometry and TEM. The bone response to Ti and Ti6Al4V implants in rabbit tibia was analyzed by a combination of histology, histomorphometry, biomechanics, SEM (back-scattered mode) and TEM analysis of the intact interface prepared by FIB.

The present results showed that the FIB *in situ* lift-out technique provided a higher quality and yield of ultra-thin samples for TEM in comparison with the *ex situ* technique. In addition, *in situ* prepared samples could be re-thinned and plasma cleaned. Commercially available dental implants showed large differences in the outermost surface layer with regards to crystallinity, morphology and thickness. Osseointegrated amputation prosthesis made of machined Ti demonstrated 75% relative bone area, 85% bone-implant contact and a direct apposition of hydroxyapatite. No difference was found between machined Ti and Ti6Al4V after 8 weeks healing time in rabbit cortical bone. In contrast, laser-modified Ti6Al4V surface had a 270% increase in torque strength and altered bone fracture pattern, correlating to an ultrastructural bonding between nanocrystalline hydroxyapatite and surface features on the micro- and nano-scales.

In summary, TEM sample preparation was successfully applied on implants, giving new information on the surface morphology and crystallinity. Limitations with the technique were: sample thickness (~100 nm) casing difficulties to analyze very thin surface layers (<10 nm) and bone-implant interfaces which were not properly bonded to sustain pre-FIB preparation. In conclusion, FIB is a new, powerful tool for sectioning ultrathin samples for subsequent TEM analysis of implant surfaces and their interfaces to bone and could be performed in combination with other techniques giving important complementary information.

Keywords: FIB, TEM, SEM, osseointegration, rabbit, human, biomaterial, titanium, titanium alloy, surface analysis, bone-implant interface, ultrastructure, surface modification, laser.

List of Papers

I. T. Jarmar, A. Palmquist, R. Brånemark, L. Hermansson, H. Engqvist, P. Thomsen, *Technique for preparation and characterization in cross-section of oral titanium implant surfaces using focused ion beam and transmission electron microscopy*, Journal of Biomedical Materials Research, In press

II. T. Jarmar, A. Palmquist, R. Brånemark, L. Hermansson, H. Engqvist, P. Thomsen, *Characterization of the surface properties of commercially available dental implants using SEM, FIB and HRTEM*, Clinical Implant Dentistry and Related Research 2008; 10(1): 11-22

III. A. Palmquist, T. Jarmar, L. Emanuelsson, R. Brånemark, H. Engqvist, P. Thomsen, *Forearm bone anchored amputation prosthesis: A case study on the osseointegration*, Acta Orthopaedica 2008; 79(1): 78-85

IV. A. Palmquist, F. Lindberg, L. Emanuelsson, R. Brånemark, H. Engqvist, P. Thomsen, *Morphological studies on machined implants of commercially pure titanium and titanium alloy (Ti6Al4V) in the rabbit*, Submitted for publication

V. A. Palmquist, F. Lindberg, L. Emanuelsson, R. Brånemark, H. Engqvist, P. Thomsen, *Biomechanical, histological and ultrastructural analyses of micro- and nano-structured titanium alloy implants: A study in rabbit,* Submitted for publication

Content

Introduction

The aim of the introduction is to give the reader an insight of the current knowledge in the field of ultrastructural analysis of the bone anchored implant surface and its interface to bone. An overview of current methods for sample preparation and analysis is provided. The basic structure of bone and its relationship to implant surfaces is supplementing a brief introduction to the term “osseointegration”.

Bone

The bone tissue is a composite material forming the skeleton, the support structure of the body. On a macro scale two types of bone tissue could be found, cortical and trabecular (Figure 1). The cortical bone, also known as compact bone, is mainly found as an outer shell of the bones. The structure is composed of osteons or Haversian systems, which are hollow circular structures with blood vessels in the center and surrounding concentric bone lamellas. The direction of the lamellas are alternated changed as rotated plywood layers[1]. Cement lines are found between the osteons, forming the border between the bone tissues. The porosity is about 5-10 %, where the contribution is Haversian channels, Volkmann’s channels (interconnecting the Haversian channels with capillaries and nerves) and lacunas (interconnected by canaliculi). The trabecular bone also known as cancellous bone is found inside the cortical bone. It is composed by plates and struts known as trabeculae. The trabeculae have a thickness of around 200 µm and are highly porous (50-95 %)[2]. The macro design is hence a sandwich construction known for it’s mechanical properties[3]. During bone formation, a third bone type, woven bone, is found, constituting an unorganized bone tissue which will gain mechanical strength during remodeling[4].

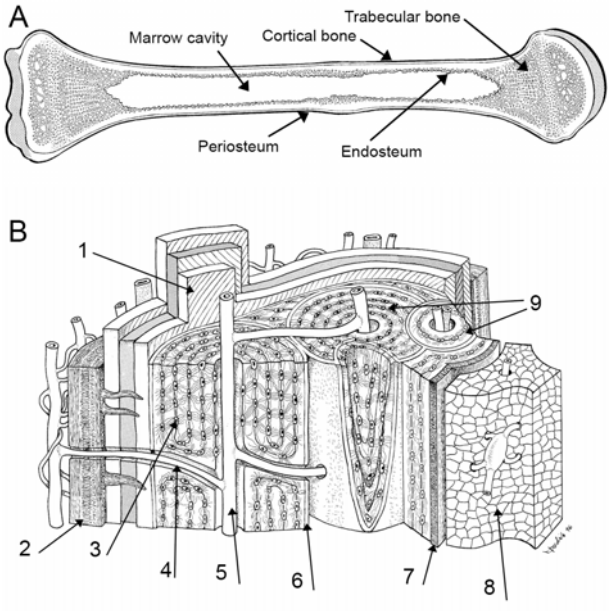

Figure 1: Schematic images of the bone structure. A) A typical long bone where the cortical and trabecular bones are represented. B) Higher magnification of the cortical bone. 1. Bone lamellas with alternating collagen directions. 2. Periosteum. 3. Osteocytes trapped in the osteons. 4. Volkmann channels. 5. Blood vessel in the center of Haversian channel. 6. The cement line separating the Haversian systems. 7. Endosteum separating the bone from the marrow cavity (8). 9. Haversian systems. (Reprinted with permission from author[5])

The bone is a living tissue undergoing constant remodeling where four cell types are involved. Osteoblasts (forming new bone), osteoclasts (dissolving old bone), bone lining cells (inactive osteoblasts at the bone surface, which could be reactivated by chemical or mechanical stimuli) and osteocytes (mature cells in the lacunae of bone tissue)[4]. It has been suggested that the osteocytes controls the remodeling by sensing the mechanical stimuli[6]. As mentioned above, cement lines are found between the osteons. Another border line is the lamina limitans, found at the bone tissue-cell interface as well as around the canaliculi. These are very similar in structure and composition, consisting of accumulations of organic material, such as proteoglycans, lipids and collagenous proteins and inorganic material such as hydroxyapatite[2,7]. Further, the third type of interface to mineralized bone would be the bone-implant interface, where as will be described later in more detail, a cement-like line has been detected between the implant and mineralized bone interface. According to Steflik et al, the canaliculi have been observed extending through the electron dense layer closest to the implant, hence able to sense the mechanical stimuli directly form the implant surface[8]. It is well established that the canaliculi traverse the cement lines[2].
On a micron scale the bone tissue is composed by an inorganic part, an organic part and water. The inorganic part is mainly hydroxyapatite, which is slightly different from the synthetic hydroxyapatite with substitute ions[9]. The organic part is mainly collagen type I, but also proteoglycans and other bone proteins. The dimensions of the collagen triple helix, fibril and the collagen bundles are 1.5 nm, 100 nm and 0.5-3 μm respectively[10,11] where the particular collagen molecules are ordered in a staggered array model (Figure 2) where a small distance between each molecule in the long direction is defined as a hole zone alternating with an overlap zone[12]. In this hollow compartment the apatite is laid down in the mineralization process of bone formation. The apatite forms as plates with the dimensions 500x250x20 Å growing in the c-axis direction[12].

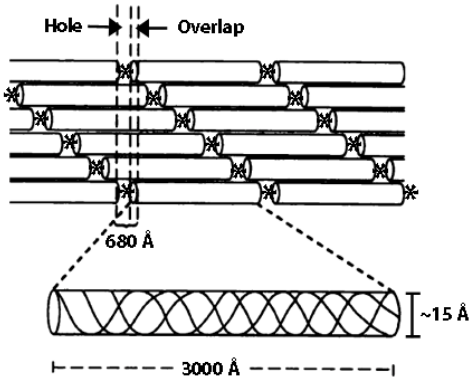

*Figure 2: Collagen molecular and fiber structure. The hole zone and overlap zone are together around 68 nm wide and give rise to the characteristic banding pattern of the tissue. The hydroxyapatite crystals * are laid down in the gaps between the collagen molecules. (Image redrawn from references [11] [13]).*

Bone healing around implants in general terms

The implant installation requires a surgical intervention which will lead to a surgical trauma as well as a foreign material is inserted in the biological environment. The biological response will depend on the surface characteristics of the implant as well as the trauma. Considering a non-toxic implant surface, the first that will happen after implantation is that the surface will be in contact with biological fluids containing proteins, salts and other bio-molecules, which will lead to protein adsorption on the surface. The remaining spaces between the implant and bone will be filled by the blood clot. Different scenarios have been suggested depending on the mechanical strength of the adsorbed molecules[14] where two different scenarios could occur, namely distant or contact osteogenesis. The difference is from where the bone is

formed and in what direction and if cells could reach the implant surface or not prior to bone apposition. For distant osteogenesis the bone forms towards the implant surface from the host bone surface, while the bone forms from the implant surface in contact osteogenesis. The difference will be the morphology of the bone-implant interface where either a cement like deposit is laid down directly at the implant surface[15] which is the case of contact osteogenesis or cells at the surface in the case of distances osteogenesis[14]. Further, it has been shown that the mechanical stimuli of the interface will alter the resulting bone formation. Excessive mechanical stimuli will result in micro motions of the interface zone which will end up in a fibrous tissue formation around the implant[16], however, the bone formation and mineralization of the interfacial tissue to implants are dependent on the local mechanical environment[17]. The proliferation and differentiation of the osteoblasts are suggested to be partly regulated by the local mechanical environment[18] and acting similar to the fracture callus formation[19].

Definitions of osseointegration

The term "Osseointegration" was first coined by Brånemark and co-workers in 1977 in conjunction with their 10 year follow up of titanium implants for edentulous jaw replacement[20]. Their definition was "The re- and new-formed bone tissues enclose the implant with perfect congruency to the implant form and surface irregularities thus establishing a true osseointegration of the implant without any interpositioned connective tissue"[20]. The definition of osseointegration has been reformulated during the years to fit the current knowledge as well as for different areas of practice and evaluation. Other definitions are "Osseointegration means a direct – on light microscopic level – contact between living bone and implant"[21], hence defining the resolution level for the definition. A subsequent definition, "A structural and functional connection between ordered, living bone and the surface of load-carrying implant"[22] incorporates the loading condition into the definition but this definition does not consider the resolution level. To the author's knowledge no definition has been made based on concluding evidence on the ultrastructural level. Definitions may serve important scientific, clinical and industrial purposes. Different definitions have been stated, however the need for new tools enabling higher resolution analyses is imperative for further understanding of the mechanisms of osseointegration.

Applications of osseointegration

The implants used could be categorized in two parts where total hip and knee replacements are in one group and dental implants, bone anchored hearing aids and amputation prosthesis are in the other group. The main difference are the surgical procedures, healing times and if the biomaterial is penetrating the skin, hence the external barrier.

The hip and knee replacement was from the beginning cemented, fixated with a polymer material in the bone and not considered as osseointegration in the same way. Today more hip implants are installed by cement-less procedures where the stem is press fitted in the medullar cavity of the femur. According to a meta-analysis of the published literature of total hip replacements no advantages was found for either fixation method[23]. Non-cemented metal arthoplasties are often associated with either a fibrous membrane or limited bone ingrowth/bone-implant contact[24-27] judged by morphological examination of retrieved, clinically well-functioning implants. On the other hand, reports of higher apposition of bone to the implant has been observed with calcium phosphate coated metal femoral stems (32-78%[28]; about 50%[29]).

Dental implants have been used since the mid 1960's[20] Observations of clinically stable oral implants, retrieved after up to 16 years showed 79-95% bone area and 56-85% bone contact[30]. The early strategy for successful treatment was to allow the biology to approach the implant, where gentle surgical technique and long healing time prior to functional loading were

important[31]. Today the strategy is to have a more aggressive implant design which will improve the early implant stability and allow faster bone ingrowth, with increased surface micro and nano topography. Also aims for improving the biological response with growth factors and cells are under development. Surface modification has been performed on dental implants the latest decade, where it has been shown that increased surface roughness, hence a larger specific area, stimulates the bone formation around implants. According to Albrektsson el al. implants could be divided into 4 different categories depending on the surface roughness value S_a. The categories are the following, smooth (S_a < 0.5 μm), minimally rough (S_a = 0.5–1.0 μm), moderately rough (S_a = 1.0–2.0 μm) and rough (S_a > 2.0 μm). It is also suggested that the moderately rough implants tend to have a better bone response compared to the others[32]. Surface roughness is one surface characteristic for a modified implant surface where other potential important factors among others are surface potential, wettability, crystalline phases and contaminations. Different methods for creating an increased surface roughness are blasting with particles, such as aluminium oxide[33,34], anodic oxidation could be used for changing the oxide structure as well as the surface topography[35-37], plasma-spraying will add material to the surface and could be done with titanium or hydroxyapatite. A more recent modification is by laser treatment which results in an increased oxide thickness and surface topography. The advantage with laser modification is that no foreign material is in contact with the implant, hence the contamination of the surface is minimal as well as the modifications could be performed on certain areas of interest without the need of masking[38,39]. It has been shown to increase the biomechanical properties of the bone-implant interface[40].

Other treatments based on the osseointegration concept have evolved from the dental implants. One is the bone anchored hearing aids which have been used since 1977[41] restoring the hearing for patient suffering from sound transmission loss from the outer ear to the inner ear.

Another more recent application is the bone anchored amputation prosthesis for lower and upper limbs which has been used since the early 1990's[42]. Recently it has been shown that the treatment increases the quality of life for amputees compared to using the traditional socket prosthesis[43]. Where some benefits are less skin irritation and pain in the remaining limb as well as increased sitting comfort[44] also an increased sensitivity of the environment is perceived through the osseoperception[45,46]. For further reading regarding the surgical procedures and rehabilitation for the patients see reference[47].

Techniques for implant surface analysis

The importance of the interactions between biological components and the surface of implanted materials has put great importance on the development of tools for surface modification and analysis. A variety of methods are designed for surface analysis. They all have their pros and cons. In the following section some of the most used analytical tools will be listed and briefly described. The tools are addressing major properties of implant surfaces, ranging from surface topography measurement via elemental analysis of the surface layer to crystalline structural analysis in transmission electron microscopy.

Surface topography

The surface topography could be measured and characterized with or without physical contact between the instrument and sample. The contact measurements use some sort of tip sliding along the surface and the vertical movement is registered along with position in the horizontal plane. The non-contact methods use light and its reflections and register the vertical position via the focus plane. For screw shaped implants the latter is preferred due to difficulties in measurement due to the macro geometry and reaching the bottom and flanks of the threads

with the contact stylus[48]. Further, for contact measurements the size and radius of the tip will determine the resolution level due to the inability to penetrate smaller cavities. Some 50 different parameters could be used for characterization of the surface structure where the parameters could be categorized in amplitude parameters, spacing parameters and hybrid parameters depending on the origin and mathematical treatment of the data[49]. The evaluation could be performed in 2 dimensions (along a line scan) or 3 dimensions (over a surface). The 3 dimensional evaluation is most suitable for implants due to eventual anisotropic surface structure, where the roughness in x and y directions are different. The most commonly used parameters in the literature for dental implants are S_a and S_{dr} which are the arithmetic average height of the irregularities and the developed surface area ratio, respectively. For further reading on this subject, the reader is referred to reviews [50,51].

Surface elemental composition

The surface elemental composition could be evaluated by auger electron spectroscopy (AES), energy dispersive X-ray spectroscopy (EDS), X-ray photon spectroscopy (XPS) and secondary ion mass spectroscopy (SIMS). The resolution level as well as the surface sensitivity differs between the methods[51]. Both AES and EDS use a primary electron beam to probe the sample, while XPS probes the sample with monochromatic X-rays. The primary electron beam interacts with the sample causing ionization. The rearrangement of the excited atoms could generate either auger electrons (used for AES) or x-rays (used for EDS) which both possess characteristic energies related to the parent atom only and not the primary electron beam which makes them suitable for elemental analysis. The auger electrons have rather low energy and could only escape from the uppermost surface layer (nm) while the x-rays could escape from higher depths (μm) making it less surface sensitive. Limitations of analysis for both AES and EDS are charging events caused by the primary beam where electrons are bombarding the sample. With XPS the charging effects are limited and the energy resolution is usually higher than for AES allowing also binding energy analysis for the individual elements in the material[52,53]. Both AES and XPS could be combined with ion etching allowing depth profiling of elements in the surface layer. The oxide thickness could also be measured by intensity relations of the oxide peak and metallic peak in the spectrum[53]. SIMS uses ion etching as a primary beam, resulting in charged secondary ion emission from the sample surface. The secondary ions are accelerated in a mass spectrometer where the charge to weight ratio could be used for identification[51]. Oxide thickness measurements of SiO_2 on silicon wafers using different techniques (XPS, AES, SIMS and TEM) showed differences in the results among the techniques, indicating the need of combining different techniques[54]. Further, it was discussed that TEM was the only technique offering a true measurement, however, only on a limited area of analysis. These techniques do not generate any information regarding the crystalline structure of the surface layer and complementary techniques are required for a more thorough analysis.

Surface phase composition

Raman spectroscopy, high-resolution TEM (HRTEM), electron diffraction and X-ray diffraction (XRD) are different techniques enabling phase identification of crystal structures. Electron and x-ray diffraction uses the phenomena where the incoming beam will be scattered in a characteristic pattern. The diffraction occurs when the orientation of the crystals fulfills Bragg's law. By angular scanning of the incoming X-ray and measurements of the diffracted X-ray the distance between the atomic planes in the crystals could be deduced. Similar results are obtained in electron diffraction in the TEM where characteristic spots are imaged in the diffraction plan. The HRTEM uses the phase contrast phenomena for imaging the fringes of the atomic columns, which could be measured and identified according to the characteristic

lattice parameter of the unit cell of the crystal structure. For TEM analysis different sample preparation methods have been used, the most commonly used is polishing and ion milling[55]. Another preparation method used is the creation of an electron transparent window by dissolution of the bulk metal leaving only the oxide layer[56,57]. The disadvantage of the latter is that the cross-section is not available where eventual gradients from the bulk metal interface toward the oxide surface could be analyzed. An advantage is that the surface area analyzed is relatively large and lateral evaluation of the oxide could be performed[56]. With Raman spectroscopy less sample preparation is needed. The technique uses the scattering phenomena of a visible light source, usually a laser with a specific wave length. The Raman scattering could be used for structural identification of an oxide layer[58,59]. However, for thin native oxides on titanium implants the degree of crystallinity and the usually thin nature of the oxide are reducing the possibility to acquire signal intensities reaching above the noise level[60].

Techniques for bone-implant interface analysis

The evaluation of osseointegrated implants are difficult in man since most of the methods are designed for retrieved implants and could therefore not be performed on implants intended to remain functional in patients. Therefore the evaluation methods could be categorized with the viewpoint of invasive or non invasive, meaning evaluation of the implant in situ (*in vivo*) or ex situ (*ex vivo*) from the patient or experimental animals. The evaluation of *in vivo* functional implants is limited to different X-ray methods and resonance frequency methods. The most common methods for evaluation of retrieved implants and its surrounding tissue include biomechanical tests, such as push or pull out or torque tests, light microscopic histological evaluation, and electron microscopy. In this part a more detailed description of the analytical methods will be given, including a description of sample preparation, analysis resolution and limitations. Since the thesis is focused on the analysis of retrieved implants only a brief introduction will be given to the *in vivo* methods.

Resonance frequency analysis

Analysis of the primary stability of an implant is an important topic as immediate or early loading of clinical implants is emerging. As described in the part of bone healing around implants, possible micro motions may lead to fibrous encapsulation and later to implant failure. The resonance frequency analysis (RFA) uses the transducer which is attached to the implant. Oscillations are induced by a piezo electric element and the responding resonance frequency is recorded. The resonance frequency is mainly determined from the marginal bone height, stiffness of the bone and the length of the transducer[61]. It has been shown that the stability increases with time, hence the remodeling of the bone-implant interface[62,63]. The RFA method has been evaluated in combination with torsional biomechanical testing and histological evaluation: the torsional testing showed significant differences in torque values between two different implant materials after 16 weeks of healing in rabbit bone[64] whereas no significant difference was detected for the RFA and histomorphometry. RFA is gaining an increased use in clinical implantology as a tool for measurement of implant primary stability, hence as an indicator for the possibilities to perform immediate and early functional loading of the implants[65].

Radiography

Radiographs are important both before and after implantation for evaluation of the host bone tissue where the implant will be implanted and the tissue reactions around the implants during the follow-up[66]. The radiographs are rather low in resolution level and some areas close to the implant can be difficult to acssess when the complete host bone is imaged. With new

micro computed tomography (μ-CT) instruments the interface could be analyzed around the whole implant and even in some cases be quantified with regards to bone area and bone-implant contact however with some artefacts due to the opaque nature of implant materials[67]. By using μ-CT on titanium coated plastic implant replicas after implantation in rabbit tibia, the analysis could be combined with TEM analysis and morphological analysis of ground sections[68]. The μ-CT is an emerging technique allowing a 3 dimensional analysis.

Biomechanics

The biomechanical evaluation of implants is designed to give a quantitative measurement of the implant stability in bone. The method could be used for comparison of different implant surface modifications or healing times. Different methods of biomechanical evaluation exist, depending on the implantation site and the direction of the measured load and have been categorized into four main types[5]:

I. Push- and pull-out tests for transcortically placed implants,
II. Push- and pull-out tests for intramedullary placed implants,
III. Miscellaneous test, which includes crack propagation, tensile tests and energy storage, and
IV. Removal torque test on rotationally symmetrical implants.

The intramedullary method is most convenient for orthopedic implants, such as total hip and total knee replacements and bone anchored amputation prosthesis which will have a load-bearing situation intramedullary in the long bones of the skeleton. For dental implants the transcortical model is more accurate as the implants are installed transcortically in either maxilla or mandible. It has been suggested that the torque test is more dependent on the bone-implant interface while the push- and pull-out test is more dependent on the surrounding bone support[69]. A drawback of the push- and pull-out tests is that most of them are performed after animal sacrifice and even after tissue fixation creating uncertainties as to the effects of post-retrieval procedures on the “true” values of the anchorage of the implant in the tissue[5].

Light microscopy

Histology and histomorphometry of tissues in relation to implanted materials (particularly hard tissues) are mainly based on fixated and resin embedded ground sections. The methodology for un-decalcified ground sections of implant and bone blocs was first described in the early 1980’s[70] and is today the most commonly used preparation method for morphological analysis of bone-implant interactions. The method consists of tissue fixation, dehydration with ethanol, resin infiltration and polymerization. The resin embedded bloc is then divided along the long axis of the implant prior to sawing a thin section which is later ground to a thin section prior to staining[70]. Important parameters are the sawing direction and the final thickness of the ground sections[71,72]. The subsequent analyses of the dyed ground sections are performed using light microscopy where detailed features of the cellular activity around the implant could be evaluated as well as quantitative and qualitative histology. A major advantage with the ground section is the possibility to have the implant material present in the section. Different polymer resins have been used and evaluated such as epoxy, methyl methacrylate and polyester[73-75]. The polymerization which most often is performed by heat treatment, UV-light treatment or by adding an accelerator to the resin will result in a hardened block. The hardness will differ between different polymers and different polymerization methods as well as the degree of polymerized monomers. An important factor is the viscosity of the resin, where resins with lower viscosities penetrate the tissue more easily.

Transmission electron microscopy

To obtain the highest resolution known today the transmission electron microscopy is needed. The resolution level is limited to the wavelength of the media used for imaging (ie. light or electrons). The visible light has per definition a fixed wavelength between 200-500 nm ranging from red to blue. The electrons have the same type of wave structure as the visible light but the wavelength is related to the speed, with higher accelerating voltage the smaller is the wavelength, hence the better is the resolution level. Another important factor for the resolution is the sample preparation, where thinner samples give better resolution due to more electron transparency and less overlapping in the view. The sample has to be less than 100 nm in order to be electron transparent, i.e. in the order of 100-200 times thinner than samples prepared by ground sectioning for light microscopy (LM). For interface analysis between implant material and biological tissue at high resolution (i.e. TEM) the sample has to be gently cut in order to withhold the information. This has been very cumbersome using the traditional methods of TEM sample preparation, such as ultramicrotome cutting where the relatively soft tissue component is easily cut while the implant part will either create artefacts as separation or breakage of the diamond knife. Several preparation techniques have been proposed in order to circumvent the technical difficulties of sample preparation:

I. The first technique, metal coated plastic plugs, used plastic replicas of implants with a thin coating of titanium which could be cut with an ultramicrotome[76].
II. By separating the implant from the tissue after embedding in resin, applying a fracture technique, the tissue adjacent to bulk materials could be further processed by cutting with an ultramicrotome[77].
III. The possibility has been explored to remove the bulk metal of the implant by electrochemical dissolution leaving the surface oxide layer and biological tissue intact for further ultramicrotome cutting[78].
IV. A recently introduced procedure of obtaining ultrathin sections using focused ion beam microscopy[79].

A detailed description of the different techniques used with some interface examples is found below. The results of published studies will later be discussed under the heading Ultrastructural analysis.

Metal coated plastic plugs

This method was described in the early 1980´s by Albrektsson and co-workers, allowing animal experimental studies of the interface between implants, even with a (thin) metal coat, and tissues (including bone)[76]. Since then different plastic resins has been used as well as different coating procedures for the metal coating and roughness parameters. In Figure 3, the general set-up is shown. In brief, after the application of a metal coat on a polymer implant, the coated plastic plug is implanted in bone tissue, allowed a certain healing period either submerged or non-submerged, harvested and removed *en bloc* with surrounding tissue, and fixated in either glutaraldehyde or paraformaldehyde. The block is then embedded in plastic resin after dehydration and possibly decalcification. Thin samples could then be cut with a diamond knife. The metal coating is thin enough enabling the cutting without breaking the ultramicrotome knife. A major advantage with the method is the possibility to analyze the intact interface between a thin metal coat and tissue. Major concerns related to this technique are the exclusion of the role of bulk properties of metal implants and the difficulty of applying surface coatings having similar chemical and textures as those found in the clinic. Hitherto, the technique has had its main benefit in basic science studies and experimental studies since the clinically used implants in bone, at least today, are based on bulk metals.

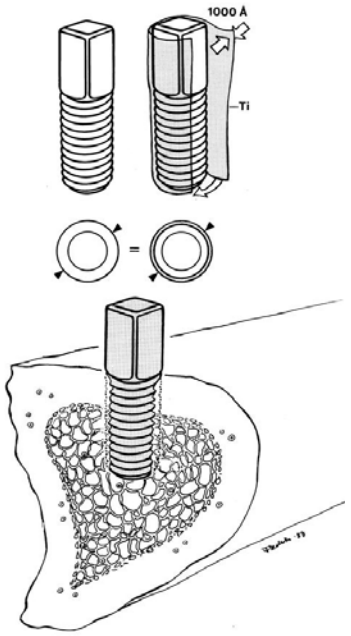

Figure 3: Schematic presentation of the plastic implant replica model. (reprinted with permission from the author)

Fracture technique

The fracture technique was introduced in the mid 1980's and the goal was to enable an ultrastructural analysis of the interfacial tissue for solid bulk metal implants from experimental as well as human clinical studies. Thomsen and co-workers implanted titanium implants (screw shaped and cylinder shaped) in rabbit tibia and femur, as well as in the abdominal wall of rats[77]. After retrieval, the implants with surrounding tissue was fixated, dehydrated and embedded in plastic resin, as described in the light microscopic section. The bloc was divided into smaller pieces by sawing prior to carefully breaking the plastic embedded interfacial tissue from the implant using a dissection microscope. The un-decalcified tissue part was then re-embedded in plastic resin prior to ultramicrotome cutting. Surface spectroscopy analysis of the implant after separation show only low quantities of tissue/plastic resins residues on the implant surface and it was concluded that the method allows ultrastructural studies of the true interface zone[80]. The surface sensitivity of the auger electron spectroscopy was in the order of 10 nm in depth, hence able to detect mono-layers of organic residues. Since then, different methods for separating the implant for the surrounding tissue have evolved. Murai and co-workers, divided the fixated and decalcified tissue and implant with a razor blade. The part where the implant remained was left in ethylenediamine tetraacetic acid (EDTA) solution during 1-2 days when finally the implant detached from the tissue. The tissue was post-fixated, dehydrated and embedded in plastic resin prior to ultramicrotome cutting[81]. Other method employed for separating the tissue from the implant is cryofracture[82]. It consists of following the established fixation,

dehydration and embedding technique and dividing the cured bloc in half prior to alternately immersing it into liquid nitrogen and water causing a fracture of the implant from the tissue[83] or in boiling water[82]. After re-embedding of the tissue part, ultramicrotome sectioning was performed. Some discussion regarding defining the actual interface tissue when the implant is broken away could be at least partly solved by sputter-coating a thin gold layer on the interfacial tissue after separation but prior to re-embedding[84].
The technique has the advantage that true experimental and clinical implants and its interfaces to bone could be analyzed. However, the method is built on the idea of creating a controlled fracture of the interface between the surface oxide and the innermost biological components of the interface, leaving uncertainties as to where the exact border between implant and tissue exists. The method also requires special set-ups and is usually confined to a few laboratories.

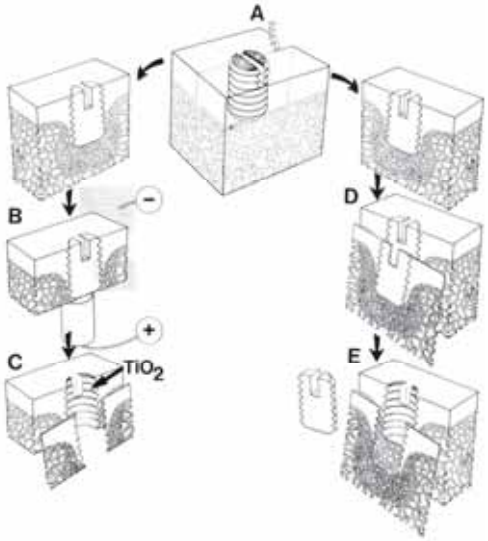

Figure 4: Schematic presentation of the fracture technique and the electrochemical dissolution of the bulk metal prior to ultramicrotome sectioning. A) Cutting the embedded implant bloc in half. B) Electrochemical dissolution of the bulk metal. C) Cutting the bone-titanium oxide interface with the ultramicrotome. D) Sectioning the implant-bone bloc prior to fracture. E) Fracturing the interfacial bone from the implant leaving the tissue ready for ultramicrotome sectioning. (reprinted with permission from author [84])

Electrochemical dissolution of the bulk metal

Electrochemical dissolution of the bulk metal was introduced in the late 1970's in order to be able to make ground sections of calcified tissue and implant for LM analysis of dyed section[85]. Later it was used for implant surface analysis, where electron transparent windows were prepared for crystallographic and morphological analysis[56,57]. By using this method for dissolving the bulk metal while leaving the oxide layer the intact bone-implant interface could be sectioned with the ultramicrotome. The methodological development was during many years focused on preparing the interface between bone and metals[30,84]. However, during this work it was concluded that the electrochemical dissolution also induced an artefactual demineralization of the bone tissue closest to the implant interface (within microns from the surface oxide)[84]. Therefore this method has been of limited value for the analysis of bone-implant interfaces. In contrast, the technique was found to be extremely valuable for the ultrastructural analysis of cells and proteins in association with metal implants in soft tissues[78].

This technique has today a limited value for bone-implant studies. Its unique potential for resolving the fine structure of metal-soft tissue interfaces has been convincingly demonstrated in experimental and clinical studies using different types of materials[86-89] The technique is due to its set-up however limited to a few laboratories.

Focused Ion Beam Microscopy

Focused ion beam microscopy was developed some decades ago, and is foremost used in the microelectronic and semi-conductor field. However the number of instruments is rapidly increasing around the world and new applications are discovered[90]. A basic FIB instrument is built up of a liquid metal ion source (LMIS), ion column, vacuum chamber, detectors, gas injection system (GIS) and an adjustable sample stage. For a more powerful tool an electron column may be added, hence a dual beam system, which allows imaging during sputtering as well as decreasing charging effects[91]. A schematic presentation of a dual beam instrument is found in Figure 5.

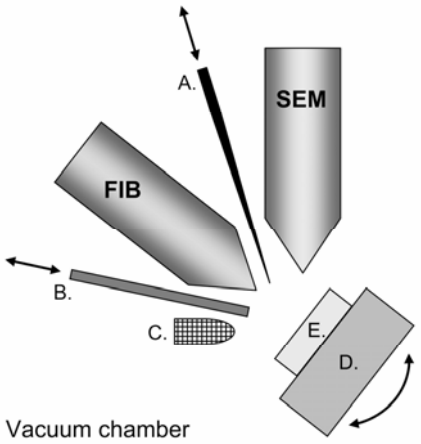

Figure 5: Schematic drawing of a dual-beam instrument. FIB represents the ion column and SEM represents the electron column. The columns are separated by 52°. A) Tungsten needle, micromanipulator system, movable in x, y and z direction. B) Gas injection system (GIS) movable in the z direction. C) The detector. D) Sample stage, possible to rotate and tilt. E) Sample.

The ion-solid interaction when bombarding a sample with gallium ions are complex, but it has been shown that the resulting sputter effects of sample material due to the ion bombardment are mainly created of elastic scattering[92]. The effects of the material in contact with the sputtered material are both a local increase in temperature and amorphization. The heating effect has been shown to be negligible due to the short dwelling times when the ion beam is rastered over the surface[92]. The effect of amorphization has been shown to be in the order of 20 nm when using a rather high beam current[92] and will be reduced with reduced beam current. The amorphization is also material dependent where silicon is affected but cupper is unaffected by this phenomena[90]. The amount of ion implantation in the sample due to ion bombardment is related to the inclination angle of the beam, where a perpendicular beam induces the most ion implantation[92]. Further, the ion beam could be used for micro and nano fabrication when performing an ion assisted chemical vapor deposition (CVD)[93]. By depositing a metal or carbon coating on the material, a protection from the ion bombardment is created. This could be used for protection of an area of interest when using the ion-solid interactions for preparing ultrathin lamellas. Hence, one important application of the FIB is the transmission electron microscopy sample preparation of ultrathin electron transparent

lamellas with a thickness of less than 100 nm[94]. Different modes of sample preparation are possible in the FIB instrument[95] and most employed are the two lift-out techniques, *in situ* and *ex situ*[96]. The FIB technique has been of limited use in the biomaterial field and mostly concerns the teeth and teeth-dental filling material interfaces[97-103]. Some initial work has been done on the bone response to implant materials[79,104-107] showing promising results. However, a need for further exploring and improving the technique is essential.

TEM basics

The basics of transmission electron microscopy is that a highly accelerated focused electron beam passes through the sample, creating an image with contrast differences due to differences in sample thickness (mass-thickness contrast), atomic number (z-contrast), crystal orientation (diffraction contrast) and interference of the waves (phase contrast). The instrument consists of an electron source, condenser lenses, condenser aperture, objective lenses, objective aperture, selected area aperture and collecting lenses. The image is viewed on a fluorescence screen. The entire system is under high vacuum avoiding interactions between the electrons and gas molecules. When the electrons pass through the sample different interactions could occur (Figure 6) which could be used for elemental analysis, crystallographic analysis as well as imaging with different contrasts.

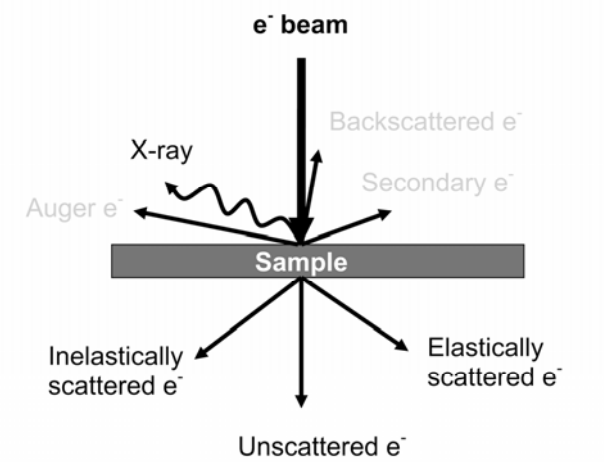

Figure 6: Schematic drawing of the different interactions that could occur when an electron passes through a material. In grey are the interesting interactions for SEM and AES. In black are the interesting interactions for TEM.

The different analytical possibilities are bright field (BFTEM), where the unscattered and some of the inelastically electrons are used for imaging, dark field (DFTEM) where certain elastically scattered electrons are chosen for imaging. By applying different objective apertures different types of DFTEM could be performed, highlighting different crystallographic directions where the contrast differences for different interests could be altered. With electron diffraction the crystallographic structure could be identified due to the characteristic scattering depending on the geometries of the unit cells following Bragg's law. Different techniques for diffraction are selected area electron diffraction (SAED) where a larger area is analyzed and convergent beam electron diffraction (CBED) where a highly focused beam is used for limiting the area of analysis. By using an instrument equipped with scanning coils, the analysis could performed in scanning transmission electron microscopy (STEM) mode, where EDS analysis could be performed on a very focused area. Further, in STEM mode high-angular annular dark field (HAADF) could be performed giving extra

contrast differences. Instruments could be equipped with energy filters enabling analysis of energy resolved spectrums of the inelastically scattered electrons such as electron energy loss spectroscopy (EELS) and energy filtered (EFTEM) analysis. In high resolution (HRTEM) crystallographic information could be gathered due to the phase contrast, where lattice fringes could be imaged and measured, revealing the interplanar distances of the unit cell. By using the described techniques, morphological, structural, elemental and molecular information could be obtained. This part was taken from the following references which are suggested for further reading[108,109].

Interface analysis

For the literature review the search has been limited to titanium and titanium alloy implants. Results from other materials will be discussed briefly.

Light microscopy

On the light microscopy level many studies have been performed on animal experimental implants as well as clinically retrieved implants. Different surface modifications, animal models, healing periods and loading conditions have been evaluated. In comparison with machined implants, the results show a tendency for higher bone-implant contact but not bone area for surface modified implants, e.g. hydroxyapatite coatings, anodic oxidation or blasting[50,110,111]. When comparing machined implant from titanium and Ti6Al4V, the results of most studies suggest no difference in the qualitative and quantitative histology[64,112-114]. However, significant differences have been reported with higher bone-implant contact and a higher degree of mineralized interface for c.p. titanium compared to Ti6Al4V[115].

Transmission electron microscopy

For titanium implants and titanium coated implant replicas some 40 published articles have been found (using Pubmed, and back-tracking the reference lists of the Pubmed publications) where the majority of articles are original publications. The interfaces described differ between the different preparation methods and between different authors/research teams and could be categorized in some typical interfaces. In Tables 1, 2 and 3, the articles concerning plastic implant replicas, fracture technique and other techniques are described with respect to implant types, species, implantation times and mode of fixation and embedding. The corresponding interfaces (A-G in Table 1-3) are described in detail in Figure 37. Almost all work has been performed on mineralized bone implant interfaces, while a few publications report serial sectioning along the entire implant[82] and some at very early time points in the healing process[83,116,117]. Others have evaluated non submerged implants[118], immediate loaded implants at short times[117] while a few have analyzed the interface after long follow up times of clinically retrieved implants after functional loading[30].

Taken together, the studies describe both some common denominators and differences of the bone-implant interface. The main types are, an electron dense layer at the implant surface, 20-50 nm wide, consisting of proteoglycans and glycosaminglycans followed by densely mineralized collagen bundles oriented parallel to the implant surface[8,82,119-126]. Others have also found a layer ranging between 20-50 nm closest to the implant surface, however this layer was not electron dense but rather consisting of ground substance containing proteoglycans and glycosaminglycans followed by a layer of randomly arranged collagen fibril ranging a few 100's of nm before the parallel running collagen bundles[76,127-131]. Others have found a larger non-collagenous amorphous zone (100-400 nm) in the immediate interface closest to the implant both for clinically retrieved implants and experimental implants[30,84,116,132] when using the fracture technique. Yet another interface was

described as a electron lucent layer (30-60 nm) closest to the implant surface followed by an electron dense layer (100-200 nm) before the mineralized bone tissue[133]. The most commonly described observation is the different layers in the nanometer range at the immediate interface to the implant, sometimes electron dense, sometimes electron lucent and sometimes a combination of both. Only a few articles describe a direct contact between the implant surface and the mineralized bone, where the collagen was reaching the surface[118]. A few publications employing electron microscopic immunocytochemistry have been performed using antibodies for osteopontin and osteocalcin[134] and cathepsins B and D[135]. Both an electron dense zone and an amorphous zone (20-50 nm) were found at separated areas in the interface zone. The immunocytochemical findings suggest that the distributions of osteocalcin and osteopontin differ between the different interface types where osteocalcin was predominantly found in the amorphous layer while osteopontin was found in the electron dense layer[134]. The findings with the Focused ion beam technique was mineralized bone close to the surface layer with some discontinuities are present at the immediate surface, bone was growing into the pores at the surface[106,107]. The discontinuities were discussed as an amorphous layer[106,107] with references to earlier work by Murai et al[81]. However, the implant analyzed was a failed dental implant from human retrieved at the time of abutment installation due to mobility and not properly osseointegrated[106,107].

The results from the different ultrastructural investigations of titanium implants and titanium coated implant replicas are not consistent with different reported interfacial morphologies. Differences may be explained by the implantation time, embedding technique and sectioning technique. Most of the ultrastructural analyses of the titanium-bone interface have been performed on implants possessing a rather smooth surface structure, eg, machined surface or even smoother for some plastic coated implant replicas. Some of the studies have used implants with roughened surfaces, however, without quantifying the roughness, either plastic implant replicas of a plasma-sprayed implants[118], implants which have been etched prior to implantation[8,82,119-126] or anodically oxidized implants[106,107]. The bone response to other implant materials, such as gold, stainless steel, zirconium and Ti6Al4V using the plastic implant replica technique with sputtered coatings of a few hundred nm showed larger interposed layers compared to pure titanium coating[76,127,128,130]. Other found no differences on the ultrastructural level between titanium and alumina implants while a difference was seen on the light optical level with better bone response to titanium[8,82,119-126]. Yet another study performed on implant made of pure titanium, Tivanium®, Vitallium® and stainless steel showed no particular structural features which differed between the materials on the ultrastructural level[136]. Hydroxyapatite implants and hydroxyapatite coated implants have been analyzed on the ultrastructural level by many authors. The typical interface is to have an apatite layer closest to the implant[105,137-139] as seen for bioactive ceramic implant materials, such as bioglass[140].

Taken together, the species, healing period, type of bone, loaded or unloaded, technical details such as decalcification or not, and implant properties (chemistry, topography) appear to play an important role for the description of the interface between metal and bone. Most likely, the technique of preparation of the ultra-thin sections for transmission electron microscopy has a crucial role. This assumption has led to the focused effort in this thesis to develop a procedure for the preparation of an intact interface between metal implants and un-decalcified bone, having the metal and oxide present in the ultra-thin section, trying to exclude the uncertainties of the role of bulk properties of the metal and the presence of the implant surface in relation to cells and extracellular matrix.

Authors and references	Bulk polymer	Ti coating thickness	Species	Time	Fixative	Fixation	Post-fixative	Decalcification	Contrast	Embedding resin	Interface
Albrektsson et al, 1982 [76]	Polycarbonate	200-300 nm	Rabbit	3 months	Glut	Immersion	Osmium tetroxide	Yes/No	UL and La, Ru	Spurr's medium	A
Linder et al, 1983 [131]	Polycarbonate	120-250 nm	Rabbit	3 months	Glut	Immersion	Osmium tetroxide	Yes/No	UL and La, Ru	Spurr's medium	A
Albrktsson et al, 1985 [128]	Polycarbonate	100 nm	Rabbit	6 months	Glut	Immersion	Osmium tetroxide	Yes/No	UL and La, Ru	Spurr's medium	A
Albrektsson et al, 1986 [127]	Polycarbonate	100 nm	Rabbit	3 months	Glut	Immersion	Osmium tetroxide	Yes/No	UL and La, Ru	Spurr's medium	A
Johansson et al, 1989 [130]	Polycarbonate	100 nm	Rabbit	3 months	Glut	Immersion	-	-	UL	-	A
Brunette et al, 1991 [141]	Epoxy	50 nm	Rat	1 to 10 weeks	Glut	Perfusion	Osmium tetroxide	No	UL	Epon	B
Listgarten et al, 1992 [118]	Epoxy	90-120 nm	Dog	3 months	Karnov-sky	Perfusion	Osmium tetroxide	Yes/No	UL	Epoxy or Spurr's medium	B
Ayukawa et al, 1996 [142]	Epoxy	50-100 nm	Rat	4 weeks	Glut and formalin	Perfusion	Osmium tetroxide	Yes	UL and La, Ru	Epon	A
Ayukawa et al, 1998 [135]	Epxoy	50-100 nm	Rat	4 weeks	Glut and formalin	Perfusion	Some with Osmium tetroxide	Yes	UL and gold	Epon or LR White	A
Okamat et al, 2007 [133]	Acrylic	150-250 nm	Rat	4 weeks	Glut and formalin	Perfusion	Osmium tetroxide	Yes	UL	Quetol 651	C
Morinaga et al, 2008 [68]	Acrylic	150-250 nm	Rat	1, 3, 5, 7, 14 and 28 days	Glut and formalin	Perfusion	Osmium tetroxide	Yes	UL	Quetol 651	-

Table 1: Studies using plastic implant replicas are listed with detailed description of implant bulk materials and thickness of the coating, also the species, implantation time, mode of fixation and contrasting. All ultrathin sections were prepared by ultramicrotome sectioning. UL is Uranyl acetate and Lead citrate. Ru, La are ruthenium red and Lanthanum. Glut=Glutaraldehyde

Authors and references	Implant form	Species	Time	Fixative	Fixation	Post-fixation	Decalci-fication	Contrast	Embedding resin	Method	Inter-face
Thomsen et al, 1985 [77]	Screw shaped	Rabbit	3, 6 and 9 weeks	Glut	Immersion	Osmium tetroxide	Yes	UL	Epoxy	Broken away under a dissection microscope	A
Linder et al, 1985 [143]	Cylinder shaped	Rabbit	3-4 weeks	Glut	Immersion	Osmium tetroxide	Yes	-	Epoxy	Fracture	A
Linder et al, 1989 [136]	Cylinder shaped	Rabbit	4 and 19 months	Glut	Immersion	Osmium tetroxide	Yes	UL	Epoxy	Fracture	A, G
Sennerby, 1991 [30]	Screw shaped	Human	1 to 16 years	Formalin or Glut	Immersion	Osmium tetroxide	No	Some with UL	LR White	Broken away under a dissection microscope	D
Sennerby, 1992 [84]	Screw shaped	Rabbit	12 months	Glut	Perfusion	Osmium tetroxide	No	Some with UL	LR White	Broken away under a dissection microscope	D
Steflik, 1992 [124]	Root or Blade shaped	Dog	5 months	Glut	Perfusion	Osmium tetroxide	No	No	Epoxy	Cryofracture	E, F
Steflik 1992 [122]	Root or Blade shaped	Dog	5 months	Glut	Perfusion	Osmium tetroxide	No	No	Epoxy	Cryofracture	E, F
Steflik 1992 [82]	Root or Blade shaped	Dog	5 months	Glut	Perfusion	Osmium tetroxide	No	UL	Epoxy	Cryofracture	E, F
Sennerby, 1993 [116]	Screw shaped	Rabbit	3, 7, 12, 28, 42, 90 and 180 days	Glut	Perfusion	Osmium tetroxide	No	UL	LR White	Broken away under a dissection microscope	D
Steflik 1993 [125]	Root and Blade shaped	Dog	5 and 11 months	Glut	Perfusion	Osmium tetroxide	No	No	Epoxy	Cryofracture	E, F
Steflik 1993 [123]	Root and Blade shaped	Dog	5 and 11 months	Glut	Perfusion	Osmium tetroxide	No	UL	Epoxy	Cryofracture	E, F
Serre et al, 1994 [144]	Screw shaped	Human	7-20 months	Glut	Immersion	No	No	UL	PMMA	-	A, B

Table 2: Studies using the fracture technique are listed with detailed description of implant geometry, species used, implantation time, mode of fixation and contrasting. All the sections were prepared with ultramicrotome sectioning. UL stands for Uranyl acetate and Lead citrate, Ru and La are ruthenium red and Lanthanum. Glut=Glutaraldehyde

Authors and references	Implant form	Species	Time	Fixative	Fixation	Post-fixation	Decalcification	Contrast	Embedding resin	Method	Inter-face
Steflik 1994 [126]	Root and Blade shaped	Dog	5, 11 and 17 months	Glut	Perfusion	Osmium tetroxide	No	UL	Epoxy	Cryofracture	E, F
Steflik et al, 1994 [8]	Root and Blade shaped	Dog	5, 11 and 17 months	Glut	Perfusion	Osmium tetroxide	No	No	Epoxy	Cryofracture	E, F
Murai et al, 1996 [81]	Cylinder shaped	Rat	28 days	Glut and formalin	Perfusion	No	Yes	UL	Epoxy	Separation during decalcification	A, E
Thomsen et al, 1997 [132]	Screw shaped	Rabbit	1 and 6 months	Glut	Perfusion	No	No	UL	LR White	Broken away under a dissection microscope	D, E
Larsson et al, 1997 [145]	Screw shaped	Rabbit	7 and 12 weeks	Glut	Perfusion	Osmium tetroxide	No	UL	LR White	-	D
Steflik et al, 1997 [119]	Root and Blade shaped	Dog	5 - 29 months	Glut	Perfusion	Osmium tetroxide and RU	No	UL	Epoxy	Cryofracture	E, F
Takeshita et al, 1997 [146]	Cylinder shaped	Rat	28 and 730 days	Glut and formalin	Perfusion	Osmium tetroxide	Yes	UL	Epoxy	Separation during decalcification	E, F
Steflik et al, 1998 [120]	Root and Blade shaped	Dog	5 - 29 months	Glut	Perfusion	Osmium tetroxide and RU	No	UL	Epoxy	Cryofracture	E, F
Ayukawa et al, 1998 [134]	Cylinder shaped	Rat	14 and 28 days	Glut and formalin	Perfusion	-	Yes	UL and colloidal gold	Acrylic	Vibration fracture	A, E
Steflik et al, 1999 [121]	Root and Blade shaped	Dog	5 - 29 months	Glut	Perfusion	Osmium tetroxide and RU	No	UL	Epoxy	Cryofracture	E, F
Futami et al, 2000 [83]	Cylinder shaped	Rat	1 - 28 days	Glut and formalin	Perfusion	Osmium tetroxide	Yes	UL	Epoxy	Cryofracture	A
Meyer et al, 2004 [117]	Screw shaped	Mini-pig	1, 3 and 14 days	Glut	Immersion	No	No	UL	Araldite	-	B

Table 2:Continuing

Authors and references	Implant form	Species	Time	Fixative	Fixation	Post-fixation	Decalci-fication	Contrast	Embeddin g resin	Sectioning technique	Inter-face
Albrektsson et al, 1981 [21]	Screw shaped	Human	5 to 90 months	Glut	Immersion	No	No	UL	Epoxy	Oblique cutting	B
Sennerby et al, 1991 [30]	Screw shaped	Human	1 to 16 years	Formalin or Glut	Immersion	Osmium tetroxide	No	Some with UL	LR White	Electropolis hing	D
Sennerby et al, 1992 [84]	Screw shaped	Rabbit	12 months	Glut	Perfusion	Osmium tetroxide	No	Some with UL	LR White	Electropolis hing	D
Sennerby et al, 1993 [116]	Screw shaped	Rabbit	3, 7, 12, 28, 42, 90 and 180 days	Glut	Perfusion	Osmium tetroxide	No	UL	LR White	Electropolis hing	D
Giannuzzi et al, 2005 [106]	Screw shaped	Human	-	-	-	-	-	-	No	FIB	A
Giannuzzi et al, 2007 [107]	Screw shaped	Human	-	-	-	-	-	-	No	FIB	A
Engqvist et al, 2006 [79]	100 nm HA coating	Rabbit	6 weeks	Glut	Perfusion	Osmium tetroxide	No	UL	LR White	FIB	B
Hemmerlé et al, 1996 [147]	Ti plasma sprayed	Human	6 months	Glut and formalin	Immersion	-	No	-	Epoxy	Sawing and grinding	B, G
Leize et al, 2000 [148]	TiH plasma sprayed	Human	14 – 40 months	Glut and formalin	Immersion	Osmium tetroxide	No	UL	Epoxy	Sawing and grinding	B, G
Hansson et al, 1983 [129]	Review										
Albrektsson et al, 1987 [149]	Review										
Ericson et al, 1991 [150]	Review										
Linder et al, 1992 [151]	Review										
Albrektsson et al, 1994 [152]	Review										

Table 3: Detailed description for the articles using different sectioning technique than plastic implant replicas and fracture technique. Also some review papers concerning ultrastructural interface analysis of the titanium-bone interface. Glut=Glutaraldehyde

Aims

The general aim of this thesis was to evaluate and optimize a novel technique for the preparation of ultrathin samples of implant surfaces and its interface to bone for subsequent transmission electron microscopy analysis.

The specific aims of this thesis were:

- To compare different protection and preparation methods in FIB with regards to sample yield and quality.

- To explore the possibilities and limitations of the FIB with regards to implant surface characterization of clinically used c.p. titanium implants from different manufacturers.

- To evaluate the FIB on clinically retrieved machined c.p. titanium amputation prosthesis in combination with histological analysis.

- To evaluate the effect of different embedding polymer resins on the bonding to machined c.p. titanium implants.

- To evaluate and compare the bone response to machined c.p. titanium and Ti6Al4V implants, including the possibilities and limits of the FIB preparation.

- To combine multiple techniques for characterization of the implant surface, biomechanical properties and ultrastructure of the interface between bone and machined and laser modified Ti6Al4V implants.

Materials and Methods

Implants

Different implants have been used in the papers. Some were test implants and others were commercially available implants from a variety of manufactures and all are listed below with corresponding paper.

Commercially available dental implants

- Fixture Original (Brånemark Integration) (Paper I, II and IV)
- TiUnite (Nobel Biocare) (Paper II)
- Steri-oss HA-coated (Nobel Biocare) (Paper II)
- OsseoSpeed (AstraTech) (Paper II)
- SLA (Straumann) (Paper II)

Commercially available orthopedic implant

- Commercially pure titanium, machined surface (Integrum) (Paper III)

Test implants

- Commercially pure titanium, machined surface (Paper IV)
- Titanium grade V (Ti6Al4V), machined surface (Paper IV and V)
- Titanium grade V (Ti6Al4V), laser modified surface (Paper V)

Surface analysis (Paper I, II, IV and V)

Scanning electron microscopy (Paper I, II, IV and V)

Scanning electron microscopy was used for evaluations of both the implant surface and the interaction with bone tissue, where detectors for secondary electrons (SE) and back-scattered electrons (BSE) were used, respectively. The different techniques, SE and BSE, offer differences in contrast and topographical information, where the SE are low energy electrons originating from the ionization process during the electron-solid interaction whereas the BSE are high energy electrons from the electron beam. The analyses were carried out in three different microscopes (Leo 440 with LaB_6 filament, Leo 1550 with FEG and FEI Strata DB235 FIB/SEM with FEG). Operating voltages between 3 and 10 kV have been used for imaging.

Interference microscopy (Paper I, II, IV and V)

3-D interference microscopy (WYKO NT-2000) Veeco Instruments, Inc., New York, USA) has a vertical resolution of 3 nm and a lateral resolution of 0.5 μm. For the different studies slightly different methods were applied in order to minimize the effect of the macro design of the screw shaped implants. In paper I and II the analyzed area was 119x91 μm and correction for cylindrical shape was performed. The results were averaged for 2 scans in the bottom of the thread of each implant type. In paper IV and V different area sizes were used at three different locations of each implant type, bottom (500 μm^2), flank (2700 μm^2) and top (2200

μm^2) of the threads. The different sizes ensured minimal intervention from the macro design of the screw shaped implants. All implants were measured immediately after obtaining them from the delivery containers. When necessary the data was restored using interpolation for missing values. The parameters measured were S_a (roughness average) and S_{dr} (surface area ratio) and presented as mean values with corresponding standard errors.

Auger electron spectroscopy (Paper IV and V)

Surface analysis with auger electron spectroscopy (AES) was performed in order to analyze the purity and thickness of the surface oxide layer. The AES analysis was performed with a PHI 660 Scanning Auger Microprobe (SAM) working at 3 keV and a beam current of 360 nA. The analysis was made in 4 points in 2 different threads and the beam was defocused over a larger area for more accurate quantification. For depth profiling a 3.5 keV Ar^+ ion gun was used and the depth of sputtering was calibrated with Ta_2O_5.

Embedding resin evaluation (Paper IV)

Implants were taken from their sterile boxes as delivered. Prior to embedding, the implants were immersed in ethanol in order to mimic the actual embedding procedure. The different plastic resins evaluated were LR White (London Resin Company Ltd), Epon-Agar Resin 100 (Agar Scientific Limited) and Technovit 7200 (Heraeus Kulzer GmbH & co.) which all are commonly used for histology. The fully cured embedded implants were cut in half in the direction of the long axis of the implant by band saw (EXAKT® cutting and grinding equipment, EXAKT® Apparatebau GmbH & Co, Norderstedt, Germany). The two halves were then treated differently according to Figure 6B. One half was cemented to a supporting plate in order to get parallel surfaces prior to grinding. The other half was re-embedded in the same plastic resin as the first embedding in order to create parallel planes. The blocks were ground successively with 800, 1200 and 4000 grit paper prior to gold coating by sputtering. The evaluation was carried out in scanning electron microscopy using magnification levels between 100 and 20,000 times. The total length of the treaded cross-section as well as the length of separation between the resin and implant at the interface (Figure 6A) was measured. Qualitative evaluation of the different embedding routes was done while a quantitative evaluation was done for the re-embedded specimens.

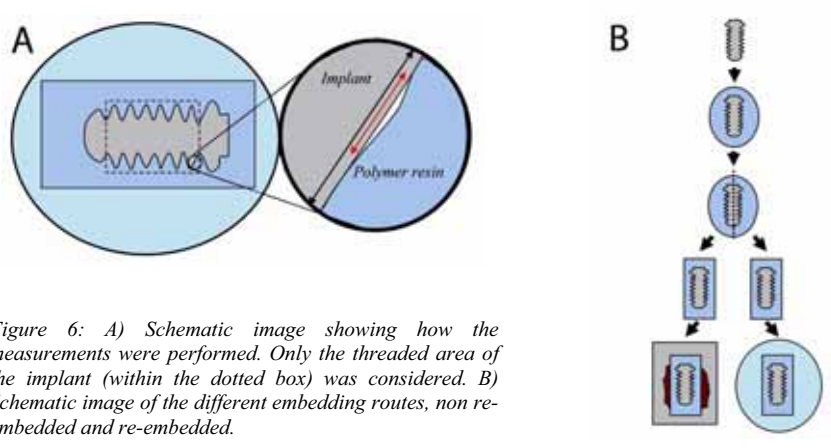

Figure 6: A) Schematic image showing how the measurements were performed. Only the threaded area of the implant (within the dotted box) was considered. B) Schematic image of the different embedding routes, non re-embedded and re-embedded.

Biological evaluation (Paper III, IV and V)

Case history (Paper III)

Male born 1934 underwent a bilateral forearm amputation in 1977 after severe trauma. The patient was treated with osseointegrated amputation prostheses in 1993. The treatment was performed in three stages: first operation, March 1993, titanium implants were placed in right ulnar and radial bone; second operation, June 1993, titanium implants were placed in left ulnar and radial bone, while percutaneous abutments were installed on the right side ulnar and radial fixtures; third operation, May 1994, percutaneous abutments were installed on left side ulnar and radial fixtures. In November 1996, the right ulnar fixture was fractured after 41 months of use caused by fatigue. The fractured outer part was removed while the still osseointegrated inner part of the implant was left in place. A custom built abutment was installed on the remaining part of the implant. In 1997, the patient developed a deep infection following the operation with the custom built abutment in the right ulnar bone. With long term antibiotics and minor revision surgery the deep infection was controlled. In June 2004, the patient was again suffering from fracture of the right ulnar implant in the junction with the custom built abutment. It was decided to remove the remaining part of the implant with a trephine after a total of 11 years of use. The implant, which was clinically stable, was immersed in formalin with the surrounding tissue. A new implant was installed in the ulnar bone and later abutment installation. At the latest patient check-up (April 28, 2008), the radiographs showed no signs of adverse effects.

Animals and surgical procedures (Paper IV and V)

Animal experimental studies were performed in paper IV and V. Ten New Zealand White female rabbits each got two implants in each leg. Experiments were approved by the Local Animal Ethical Committee, University of Gothenburg, Sweden (30606). The animals were anaesthetized prior to surgery with intramuscular injections of fluanisone (Hypnorm®, Janssen, Brussels, Belgium; 0.7 mg/kg body weight) and an intraperitoneal injection of diazepam (Stesolid®, Dumex, Copenhagen, Denmark; 1.5 mg/kg body weight). Additional fluanisone was given approximately every 20 minutes throughout the surgery which took around 2 hours/animal. The legs where shaven and disinfected with chlorhexidine and the surgery was performed under sterile conditions. The tibial metaphysis was exposed by skin incision and blunt dissection of the underlying tissues. Two holes in each tibial metaphysis (proximally and distally) were prepared by a dental guide drill and enlarged with 2 mm twist drill, pilot drill and 3.15 mm twist drill during irrigation with saline, finally the holes were tapered with a screw tap. The implants were installed according to a randomization scheme. Prior to suturing, cover screws were installed on the implants to avoid bone ingrowth in the interior threading, later used for abutment attachment for the biomechanical test. The area was rinsed with saline and sutured in separate layers with 5-0 Vicryl® and 4-0 Monocryl® or 3-0 Ethilon®. Animals were given trimetoprim 40mg + sulfadoxin 200mg/ml (Borgal® vet, Hoechst AB) prior to surgery and two days postoperatively. Analgetics, buprenorphine (Temgesic®, Reckitt and Colman, USA, 0.05mg/ml), were given during three days postoperatively. The animals were housed separately for 7 days post-operatively and in group housing for the remaining observation period.

Biomechanical evaluation (Paper V)

8 weeks after implant installation the animals were anaesthetized and the skin over the tibial metaphysis was reopened (Figure 7). The cover screw was removed and a special abutment was installed on the distal implant. A torque test machine was connected to the abutment and calibrated prior to angular torque measurement. With the particular test machine used the

torsional load could be registered using constant rotation, also the rotation could be reversed for evaluating elastic and plastic deformation of the interface zone[69]. After testing, the abutment was detached and the implants were removed *en bloc* together with the surrounding tissue and fixated in glutaraldehyde.

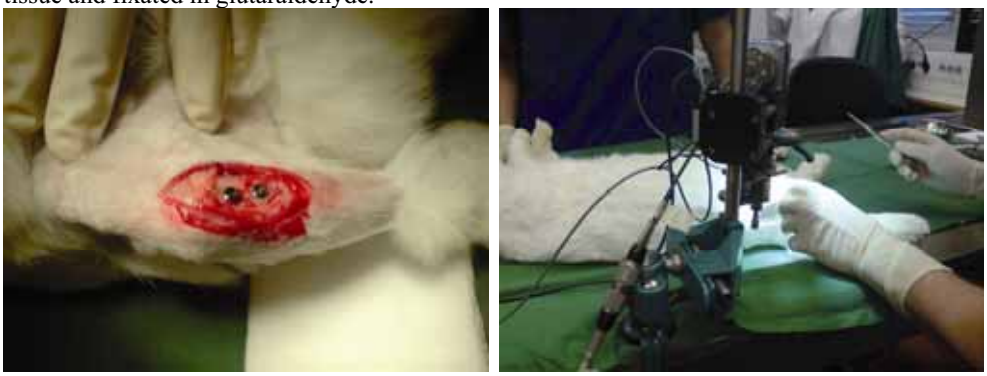

Figure 7: The skin was opened in order to access the implants, the supraperiosteal bone formation was removed prior to unscrewing the cover screws. The mechanical testing was performed on anesthetized animals.

Histological evaluation (Paper III, IV and V)

The fixated tissue-implant blocs were dehydrated in a series of graded ethanol baths prior to plastic embedding in LR White (London Resin Company Ltd) in Paper III and Technovit 7200 (Heraeus Kulzer GmbH & co.) in Paper IV and V. The curing processes were either by accelerator (LR White) or by UV-light (Technovit). The fully cured blocs were then divided along the long axis of the implant (EXAKT® cutting and grinding equipment, EXAKT® Apparatebau GmbH & Co, Norderstedt, Germany). Ground sections[70] (Figure 8) were prepared from one on the halves by sawing and grinding until thickness of 50 µm (Paper III) and 15-20 µm (Paper IV and V). The ground sections were subsequently stained with 1 % toluidine blue prior to histological evaluation using a Nikon Eclipse E600 light microscope. The quantitative histomorphometric measurements consisted of determining the bone area within the threads and the bone to implant contact along the threaded perimeter (Paper III and IV). Qualitative histology was performed on the sections for evaluating eventual adverse tissue reaction as well as the cellular response and general tissue appearance.

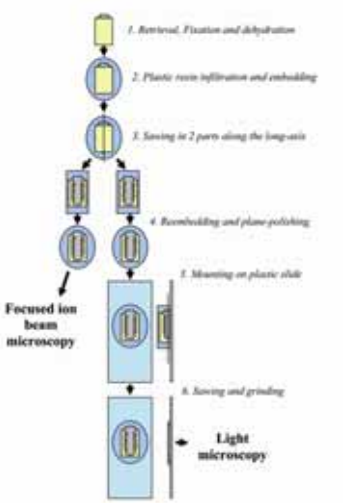

Figure 8: Schematic presentation of the sample preparation chain.

Focused ion beam microscopy (Paper I, II, III IV and V)

Sample preparation of implant surfaces (Paper I, II, IV and V)

TEM sample preparation for implant surface analysis was performed with a dual beam focused ion beam microscope (FEI Strata DB235 FIB/SEM). Two different methods for sample lift-out were used, *ex situ* (paper I and II) and *in situ* (paper I, II, IV and V). The

difference between the methods is exemplified in Figure 9, where the final thinning is performed on the TEM grid after transfer from the bulk sample or before the transfer.

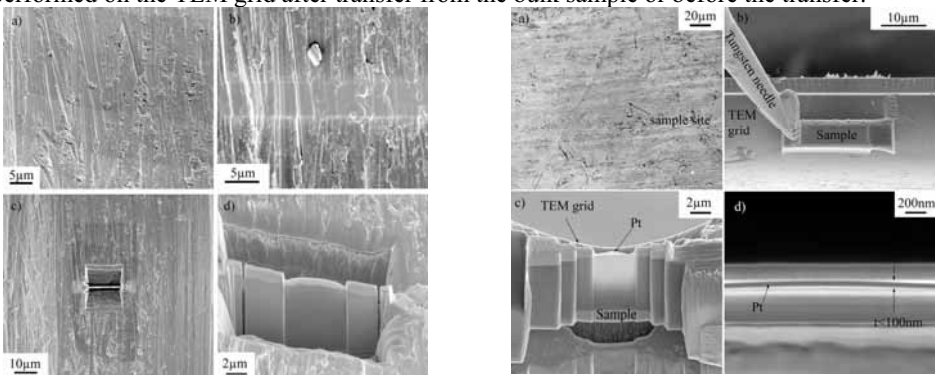

Figure 9: Images of sample preparation using ex situ (left; a-d) and in situ (right; a-d) lift-out techniques. For ex situ the rough milling and final thinning is done prior to lift-out, while for the in situ the rough milled lamella is transferred to a TEM grid prior to final thinning.

Further, three different techniques for protecting the surface of the implant have been evaluated during the thesis work: ion assisted platinum deposition, electron assisted platinum deposition followed by ion assisted platinum deposition, and plastic embedding of the implant and extracting the sample from the interface between plastic resin and implant (Figure 10).

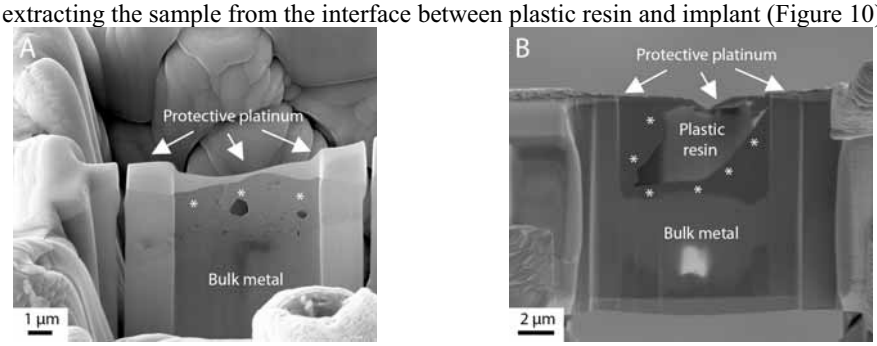

*Figure 10: SEM images of the FIB prepared samples using different techniques for protection. A) Sample taken directly from the implant surface where the surface layer was protected by the Pt deposition. B) Sample which was protected by resin embedding prior to FIB preparation. * implant surface.*

Further, different TEM grids have been used, where the sample could be attached on only one side (L-shaped) or on both sides (V-shaped) exemplified in Figure 11.

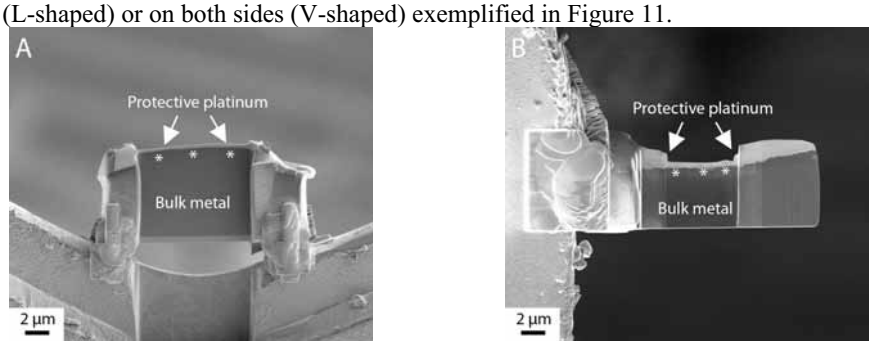

*Figure 11: SEM images of in situ lift-out FIB samples attached to the TEM grid. A) V-shaped TEM grid, sample attached in both ends. B) L-shaped TEM grid, sample attached in one end. *implant surface.*

Sample preparation of tissue-implant interfaces (Paper III, IV and V)

The counterpart of the resin embedded implant-tissue bloc was used for preparation of electron transparent TEM samples for ultrastructural analysis using the FIB. The bloc was glued upwards on a regular SEM stub by adhesive carbon tape, gold coated by sputtering and inserted in the vacuum chamber of the FIB (FEI Strata DB235). A 100 nm thick sample of the intact interface between implant and tissue was prepared using an *in situ* lift-out method. The area of interest was first protected by platinum deposition, followed by rough cutting of trenches on either side of the platinum strip. The lamella was transferred to a V shaped TEM grid for final thinning using beam currents down to 50 pA (Figure 12).

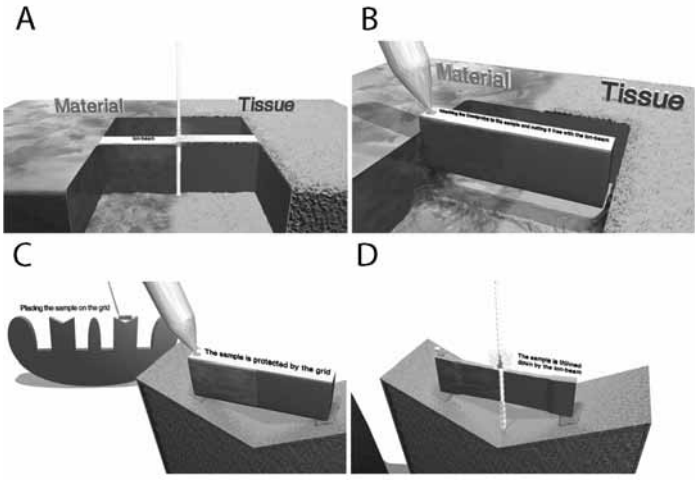

Figure 12: Schematic images of the sample preparation of tissue-implant interfaces. A) Cutting trenches at either side of the platinum protective strip. B) Attaching the micromanipulator and lift-out. C) Transfer and attachment of the sample to the TEM grid. D) Final thinning.

Transmission electron microscopy (Paper I, II, III, IV and V)

Transmission electron microscopy was performed on the FIB produced samples using 2 different microscopes (Jeol JEM 2000 FXII and FEI Tecnai F30) operating at 200 keV and 300 keV, respectively. Both microscopes were equipped with an energy dispersive X-ray spectroscopy (EDS) system allowing elemental analysis by analyzing emitted X-rays. The FEI Tecnai F30 was also equipped with an energy filter (Gatan) which allows energy resolved spectroscopy by means of electron energy loss spectroscopy (EELS) and energy filtered TEM (EFTEM). For EFTEM a three window technique was used where images of the electrons with energies just around the interesting energy were obtained and processed for eliminating the background noise. Electron diffraction was performed both as selected area electron diffraction (SAED) and convergent beam electron diffraction (CBED). SAED gives the diffraction pattern from corresponding crystals over an area defined by the aperture while for the CBED the beam is focused on a single grain.

Statistics (Paper IV and V)

Non parametric paired test (Wilcoxon Signed Rank Test) was used in order to evaluate the statistical significance between the test and control implant with regards to torque values for the biomechanical evaluation in paper V and the mean percentages from each ground section evaluated in the histomorphometrical evaluation of both bone area within the threads and bone-implant contact in paper IV.

Results

Paper I and II

Surface analysis of a selection of commercially available, oral implants was performed with a combination of different techniques, i.e. scanning electron microscopy, interference microscopy and focused ion beam with subsequent transmission electron microscopy. Further, different sample lift-out techniques were evaluated in combination with two different techniques for protecting the implant surface.

Scanning electron microscopy

The SEM analysis showed differences in macro-design. Apparent differences were also observed regarding the isotropic characteristics of the surface irregularities. The machined implant was anisotropic where the direction of the surface irregularities mainly followed the machining direction and dominated by the scratches, ridges and valleys. The surfaces of implants modified by blasting and acid etching, plasma spraying and anodic oxidizing were isotropic without a preferential direction of the irregularities. Differences in surface structure were seen at higher magnification (Figure 13) where characteristic geometries could be found. The SLA surface showed a surface roughness in two levels, macroscopic valleys and microscopic pits and craters with sharp edges. The OsseoSpeed surface demonstrated a surface structure where flakes were distributed on the surface as islands. The HA plasma sprayed surface had a more spherical structure of the surface irregularities with softer edges, occasionally pores in the µm scales was seen. Many cracks were observed on the surface but no signs of flaking. The TiUnite surface was dominated by round pores either extending from the surface as volcanoes or as holes in the surface. The size of the pores varied where the general picture was that the volcanoes showed a larger diameter (~1-12 µm) than the holes in the surface (~0.5-1 µm). The edges were rather smooth. The Original surface show scratches and ridges in the micron scale which were mainly oriented with the machining direction.

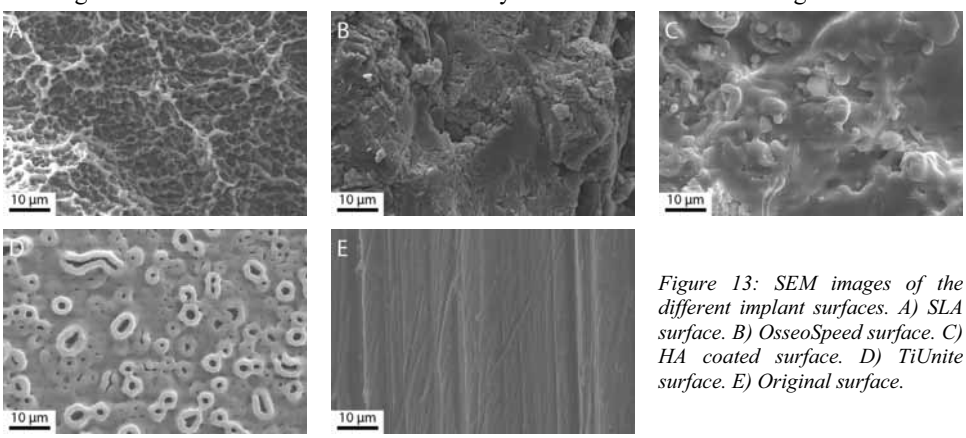

Figure 13: SEM images of the different implant surfaces. A) SLA surface. B) OsseoSpeed surface. C) HA coated surface. D) TiUnite surface. E) Original surface.

Interference microscopy

The mean S_a values measured at the bottom of the threads showed large variation between the different implant surfaces. The HA coated surface was the roughest while the original surface was the smoothest. In Figure 14 the color maps show the surface roughness in 2d and 3d. It is apparent that the lateral resolution of the interference microscopy was not enough for penetrating the porous structure of the TiUnite surface. For the other surfaces the roughness maps are comparable to the SEM images (Figure 13).

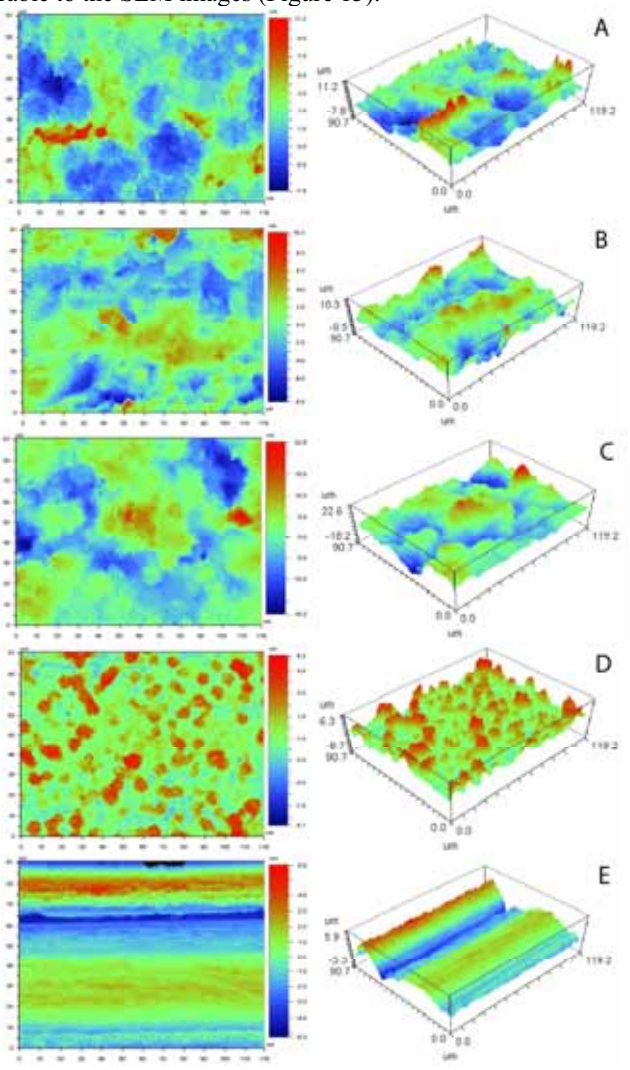

Figure 14: 2 and 3 dimensional images of the surface structure produced by interference microscopy, correction for tilt and cylinder shape have been performed. A) SLA surface. B) OsseoSpeed surface. C) HA coated surface. D) TiUnite surface. E) Original surface.

Transmission electron microscopy

TEM sample preparation of the SLA surface was difficult due to the highly irregular and sharp surface features. The platinum deposition was uneven in thickness and preferential milling of the high peaks resulted in difficulties of producing a thin sample (Figure 15). Heavy dislocations were found at the surface layer while no structure could be identified by HRTEM and diffraction.

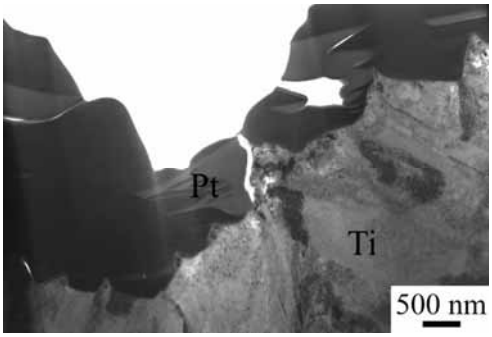

Figure 15: TEM micrograph of the SLA surface. The surface roughness is clearly visible in the sample where sharp peaks of .5-1 µm are visible while the Pt layer is irregular in thickness.

The OsseoSpeed surface possessed two levels of surface structures. Samples were prepared at the different locations in order to evaluate both surface structures in cross-section. The elevated islands consisted of a porous layer of crystalline titanium oxide composed of both rutile and anatase (Figure 16) with a thickness of 0.5-1 µm while the lower surface was found to be amorphous in structure with a thickness of 10 nm. Fluoride was detected by XPS but not in the TEM indicating a monolayer on the surface rather than incorporated in the oxide layer.

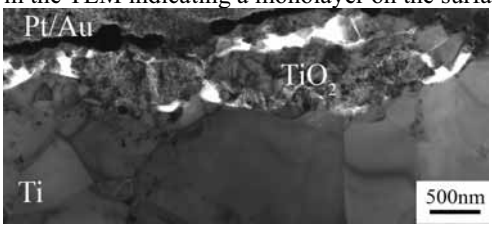

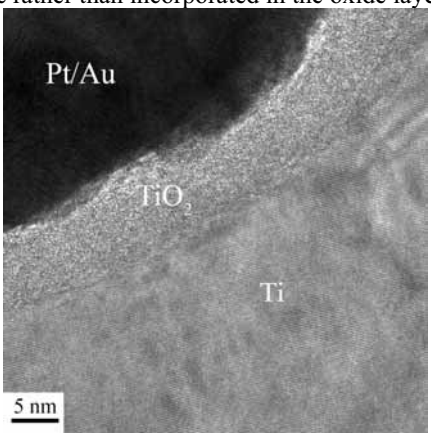

Figure 16: TEM micrographs of the OsseoSpeed surface. Left) Sample taken of elevated surface island. Right) Sample taken of at the lower surface in between the surface islands.

The HA coated implant revealed an amorphous surface layer (a few µm thick) and a crystalline subsurface layer (Figure 17). According to HRTEM the lattice parameter for the crystalline phase could be identified as hydroxyapatite. EDS analysis showed the presence of calcium, oxygen and phosphorous.

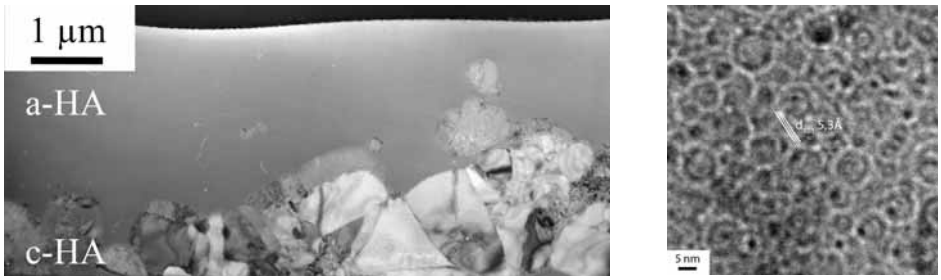

Figure 17: Left) Bright field TEM micrograph of the sample, the outermost layer is amorphous while the subsurface layer is crystalline. Right) Hydroxyapatite phase in the crystalline part is identified by HRTEM.

The TiUnite surface showed a 2-3 µm thick oxide layer (Figure 18). The layer could be divided in 2 sub-layers. Firstly, close to the bulk metal a porous interface was demonstrated, consisting of an amorphous oxide with low content of phosphorous according to EDS. Secondly, a denser layer containing crystalline grains identified as anatase by HRTEM and diffraction with amorphous oxide in between the grains. This layer possessed a higher content of phosphorous than the porous layer. The phosphorous content gradually decreased towards the implant surface which was of amorphous structure.

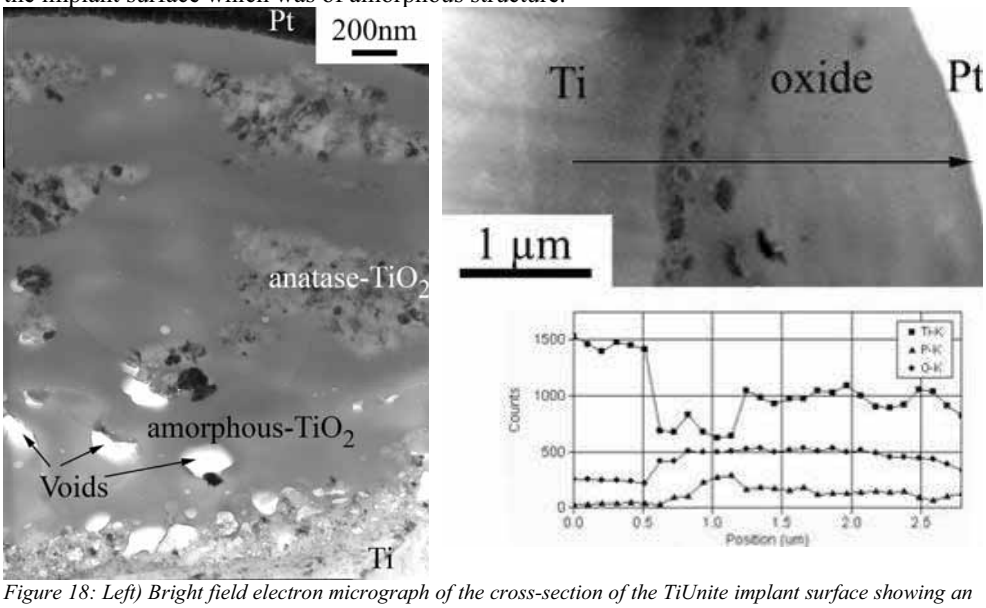

Figure 18: Left) Bright field electron micrograph of the cross-section of the TiUnite implant surface showing an amorphous oxide with crystalline grains within. The outermost layer was amorphous along the whole sample. Right) The EDS analysis in STEM mode showing presence of phosphorous in the oxide layer.

The original, machined surface showed a crystalline oxide layer with a thickness of 10 nm (Figure 19A), identified as rutile by HRTEM. Further, the platinum protective deposition was shown to be important for avoiding damage of the surface layer, where the sample only protected by ion assisted vapor deposition showed no intact surface layer, while the Pt seemed to be integrated in the bulk metal (Figure 19B). The *in situ* lift-out technique was more time consuming compared to the *ex situ* lift-out. However, the sample yield and quality was superior, in addition with the possibilities of re-thinning and plasma cleaning the *in situ* lift-out was considered the technique of choice for subsequent surface analysis in TEM.

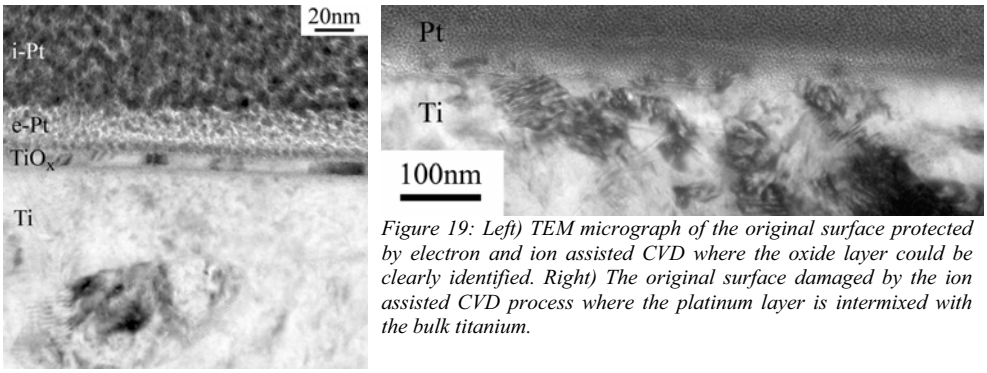

Figure 19: Left) TEM micrograph of the original surface protected by electron and ion assisted CVD where the oxide layer could be clearly identified. Right) The original surface damaged by the ion assisted CVD process where the platinum layer is intermixed with the bulk titanium.

Paper III

Histology

The inner cavity at the apical end of the implant was dominated by trabecular bone (Figure 20) surrounded by well vascularized bone marrow. Few inflammatory cells were detected. The bone trabeculae had a predominantly perpendicular direction to the long axis of the implant in the middle of the cavity while they were more aligned with the implant closer to and in contact with the surface. The threaded outer side of the implant was dominated by lamellar cortical bone which was remodeled with Haversian systems surrounded by osteocytes. The threads closest to the implant fracture were dominated by soft tissue. Many threads were completely filled with bone.

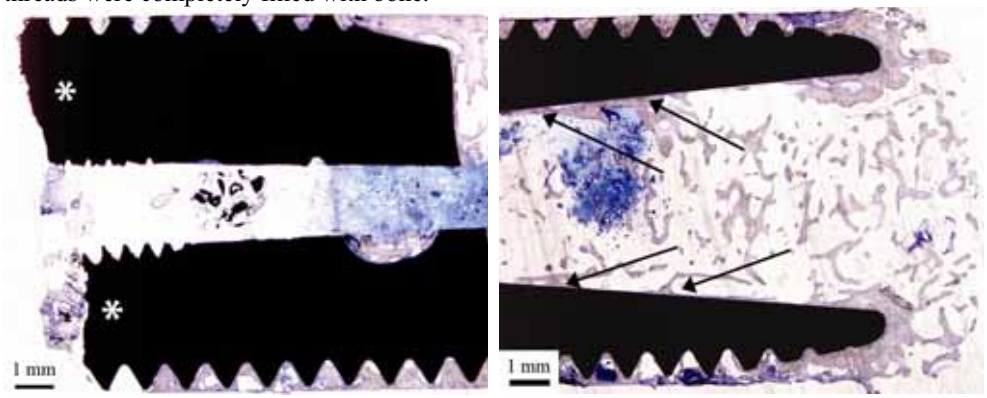

Figure 20: Light micrographs of implant and tissue retrieved from human ulnar bone after 11 years. Left: The material fracture (white stars) indicates the top of the implant, where no tissue or soft tissue dominates the first threads. Right: The apical part revealed a large amount of trabecular bone inside the hollow implant, where the bone was in direct contact with the implant (black arrows).

The quantitative histomorphometry revealed a large amount of bone tissue within the threads and in direct contact with the implant surface. An exception was closest to the implant fracture zone where the threads were dominated by soft tissue. The bone implant contact and the bone area within the threads were averaged over 59 threads excluding the 4 threads closest to the implant fracture (Figure 20), with mean values of 85 ± 2 % and 75 ± 4 %, respectively.

Ultrastructure

The interface between bone and implant was separated at large distances of the perimeter along the implant rim, reducing the number of sites for FIB sample preparation (Figure 21). Samples for FIB preparation were made at the tip of a thread.

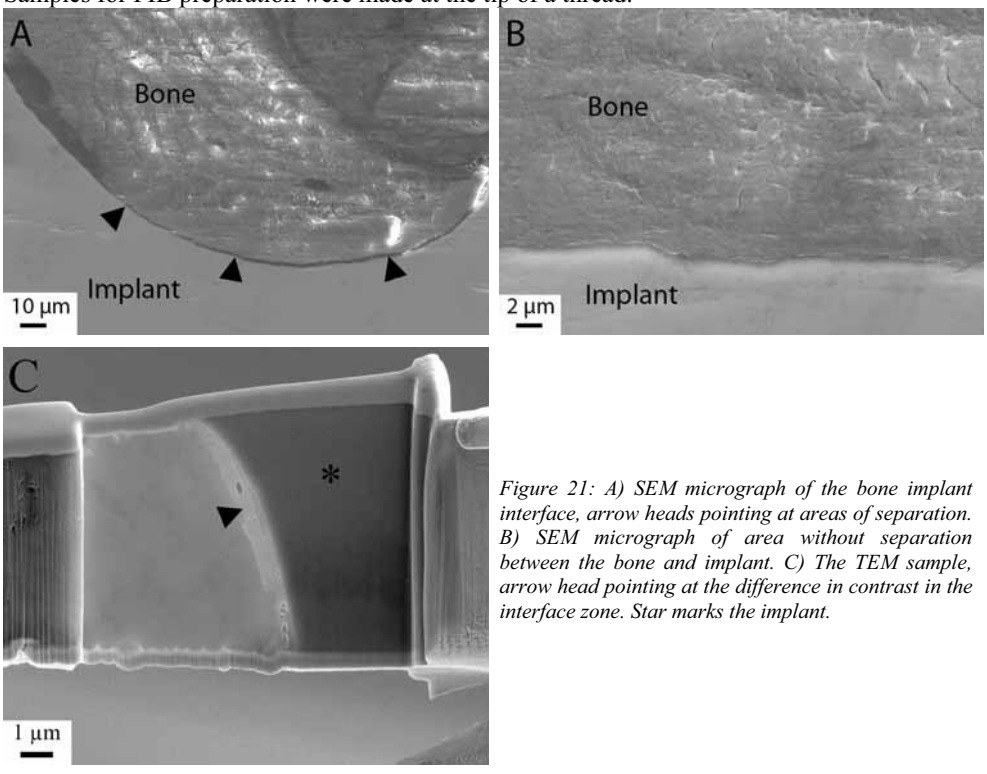

Figure 21: A) SEM micrograph of the bone implant interface, arrow heads pointing at areas of separation. B) SEM micrograph of area without separation between the bone and implant. C) The TEM sample, arrow head pointing at the difference in contrast in the interface zone. Star marks the implant.

Bright field TEM imaging of the implant-bone interface revealed an interface zone characterized by an inner about 200 nm thick apatite layer and an outer electron dense layer with high diffraction contrast (Figure 22A). Mineralized bone was identified by the characteristic collagen banding and the randomly organized hydroxyapatite crystals. An artefact was seen at the bone implant interface, showing predominance of carbon according the EFTEM, however, at the immediate implant surface a layer of calcium was found. In the high resolution mode (Figure 22C) the presence of Ca at the implant surface was confirmed to be crystalline hydroxyapatite (HA). The distance between the lattice fringes corresponded to the HA (002). Further, an amorphous layer between the crystalline titanium grains and the hydroxyapatite indicated the presence of an amorphous titanium oxide.

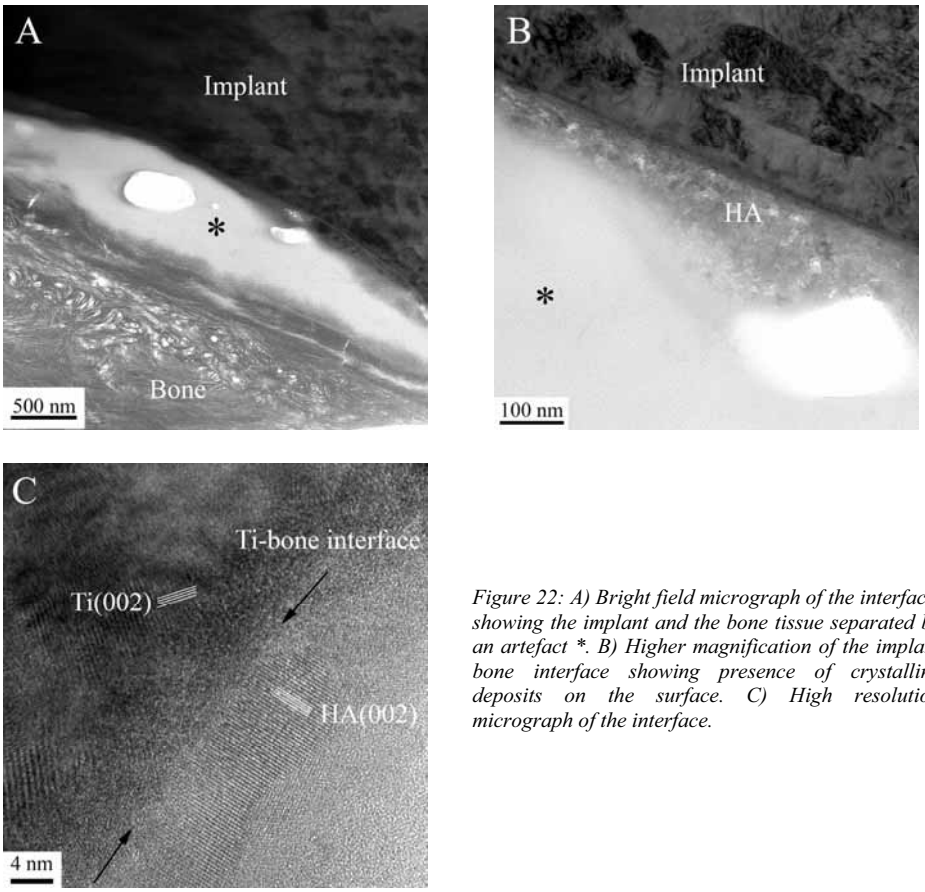

*Figure 22: A) Bright field micrograph of the interface, showing the implant and the bone tissue separated by an artefact *. B) Higher magnification of the implant bone interface showing presence of crystalline deposits on the surface. C) High resolution micrograph of the interface.*

Paper IV

Polymer resin evaluation

According to the SEM analysis no major qualitative difference was found between two different embedding routines: a similar degree of separation between implant and respective plastic resin was found. In contrast, large differences between the different plastic resins were observed. Measurements (Table 4) showed that LR White had an inferior adaptation to the implant compared to both Technovit and Epon. The width of the gap also varied among the plastic resins with the largest separation observed for LR White (200-2000 nm) compared to Epon (150-1000 nm) and Technovit (150-400 nm), however the larger cracks were sparse.

Plastic resin	A (%)	B (%)	C (%)	Mean (SE)
LR White	92.7	40.5	79.3	**70.8 (15.6)**
Epon	7.2	0.9	14.7	**7.6 (4.0)**
Technovit	15.8	2.3	1.2	**6.4 (4.7)**

Table 4: The degree of separation between the embedding resin and implant for three different resins with three samples of each resin.

Surface analysis

The surface analysis of the machined titanium and titanium alloy implants used in Paper IV was performed using a combination of different techniques in order to determine the surface topography, chemistry and morphology. Interference microscopy (Table 5) showed only minor differences in surface topography between the different implant materials. This was confirmed by SEM (Figure 23), where the surfaces were imaged at different magnifications. The surface structure consisted mainly of ordered ridges and valleys. According to the auger electron spectroscopy (AES) similar elemental composition was found on the surfaces (Table 6). The main surface elements were titanium, carbon and oxygen, a small quantity of aluminum was found on both implant materials. However, no vanadium was detected at the immediate surface. The analysis showed presence of contaminations of elements, such as calcium at higher concentrations, while phosphorous, chlorine, sodium and calcium and lead were detected at low quantities. The depth profiling showed similar surface oxide thicknesses (approximately 5 nm) for both implant types. The titanium grade V implant showed increasingly amounts of aluminum and vanadium along the depth profile. The focused ion beam prepared TEM samples were protected with plastic resin embedding prior to sectioning in order to protect the surface layer. The surface layer on both samples was approximately 10 nm and amorphous in structure (Figure 24).

	Titanium grade I		**Titanium grade V**	
	S_a (µm)	S_{dr} (%)	S_a (µm)	S_{dr} (%)
Top	0,388	18	0,333	15
Flank	0,468	21	0,390	18
Bottom	0,123	10	0,186	14

Table 6: The roughness values measured by interferences microscopy. The lower value in roughness in the bottom of the thread was related to smaller analyzed area.

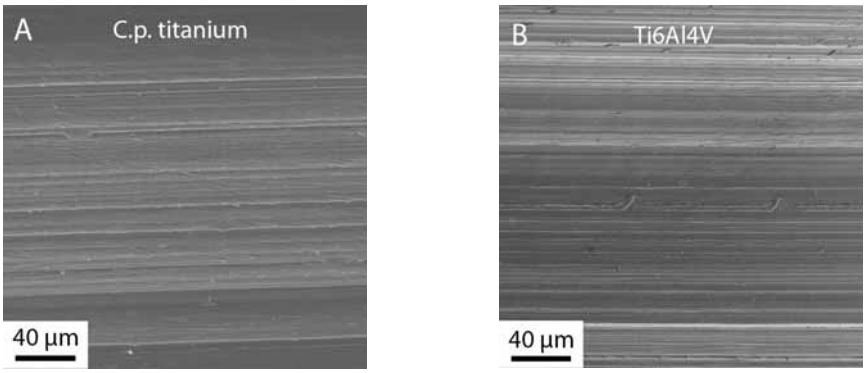

Figure 23: Scanning electron micrographs of the machined implants. A) C.p. titanium. B) Ti6Al4V.

Element	Ti	O	C	P	S	Ca	Cl	Si	Na	Al	Pb	V
C.p. titanium	9.2	31.7	38.1	0.2	1.2	12.9	2.5	0.2	1.6	2.2	0.1	0
Ti6Al4V	11.6	39.5	35.1	0	1.1	2.3	0.6	0	2.3	2.4	5.1	0

Table 6: Auger electron spectrum from the c.p. titanium and Ti6Al4V implants surfaces.

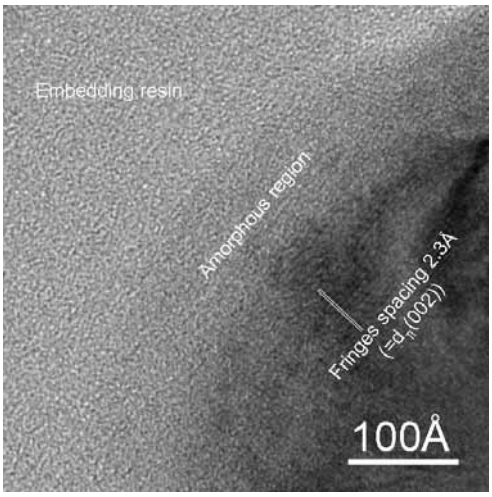

Figure 24: TEM micrographs of the surface layer of the Ti6Al4V sample. Between the crystalline grains of the bulk material and the embedding resin an amorphous layer was seen. The thickness was about 10 nm.

Histology

Histomorphometry did not reveal any significant difference between the titanium and titanium alloy implants with respect to bone-implant contact (p=0.575) and bone area within the threads (p=0.508). The mean bone-implant contact (with corresponding standard error) was 21.5 % ± 2.3 % for c.p. titanium and 20.9 % ± 2.1 % for Ti6Al4V. The mean bone area within the threads with corresponding standard error were 47.7 % ± 1.0 % for c.p. titanium and 48.7 % ± 2.0 % for Ti6Al4V. A similar histology was observed around the two implant materials. The peri-implant tissue was characterized by supra-periosteal new bone formation, new and old bone filling the threads on the level of the compacta (thread level 1-2), new bone as part of an endosteal downgrowth along the implant (thread level 3-4) and bone marrow (thread level 5-6) (Figure 25). Both at the surface of the implants and at a distance, an intense bone remodeling was ongoing. The bone which was formed superficial to the old compacta often consisted of a new compact bone layer with underlying bone trabeculae and bone marrow, in direct continuity with the surface of the old compacta. The compacta consisted of both old, lamellar bone and new bone. Within the threads of the implant, new, mineralized bone was in direct contact with the implant. The bone surfaces which were not in direct contact with the implant surface demonstrated resorption, as judged by moderately scalloped regions with the presence of osteoclasts, or appositional bone growth, as judged by the presence of osteoid and more or less ordered rims of osteoblasts. Blood vessels were either detected within the mineralized bone or in the soft tissue of the not-yet mineralized zone between the bony surfaces and the implant. Extravascular erythrocytes as an indication of bleeding were rarely detected. The endosteal bone downgrowth along the implant usually reached the 3rd or 4th thread. This portion of new bone was regularly of a lamellar character. The general histological picture in the lower threads was that of bone marrow filling the threads, often with a 2-10 cell layer thick condensation of soft tissue, with cells exhibiting a variety of morphological features, ranging from large, mesenchymal-like undifferentiated cells to osteoblasts and macrophages. Isolated bone islands were frequently observed inside the threads.

Occasional (foreign body) multinuclear giant cells were detected directly at the implant surface in the level of the lower threads. No adverse tissue reaction or inflammation was observed in the ground-sections of either implant material.

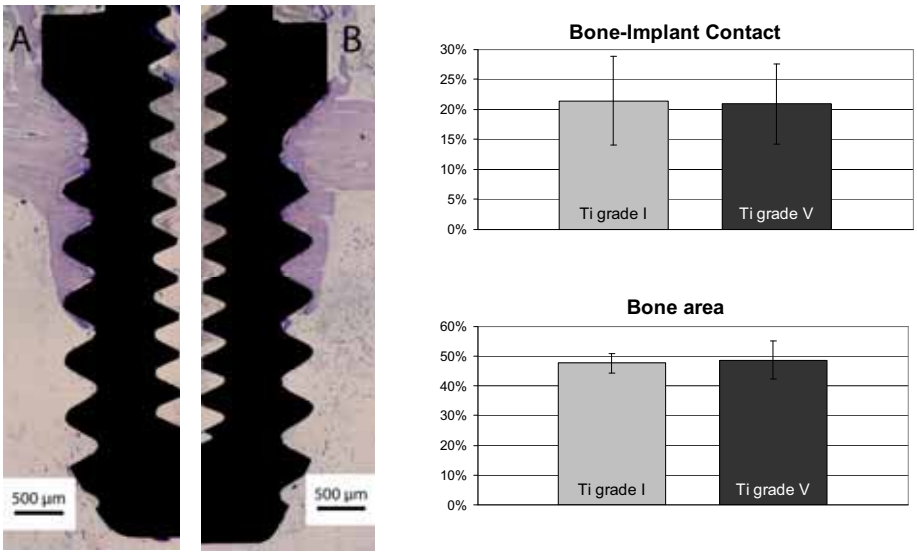

Figure 25: Light micrographs of A) C.p. titanium and B) Ti6Al4V. Histograms of the C) Bone implant contact and D) the bone area within the threads. Error bars corresponds to standard error (SE).

Focused ion beam microscopy

No intact ultrathin samples could be prepared using the FIB due to separation along the whole perimeter of the implant and bone. The separation was seen directly from above in the FIB, however, trenches were cut in order to investigate if the separation was only superficial. It was found that the separation was following the implant surface in the depth (~10-15 µm) of the bloc. Figure 26 shows two samples attached to a V shaped TEM grid, during final thinning. The separation seen was increasing during thinning due to preferential milling in the void space.

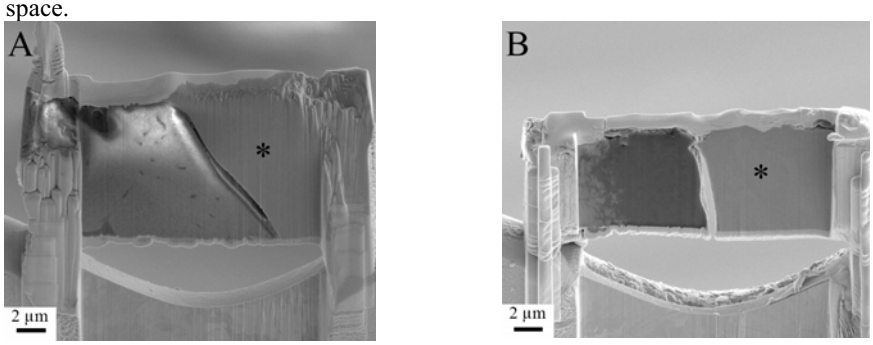

*Figure 26: Samples of the implant-bone interface attached to the TEM grid. A) Ti6Al4V implant and bone. B) C.p. titanium implant and bone. Separation is observed along the whole implant surface. * denotes the implant.*

Paper V

Surface analysis

Surface analysis of machined and laser-modified Ti6Al4V was carried out with different techniques allowing topographical, elemental and structural analysis of the surface oxide layer. The auger electron spectroscopy shows that the main elements of the surface were titanium, oxygen and carbon. A smaller amount of carbon was found in the bottom of the

threads of the laser treated surface compared to the other sites. Other elements found on the surface were calcium, sodium, potassium, aluminum, sulfur, chlorine and lead. The interference microscopy showed an increase in surface roughness for the laser treated surface compared to the machined implant at the top and flank of the threads. No roughness value could be gathered at the bottom of the thread due to shadowing effects for the roughness. The increased surface roughness was confirmed by SEM (Figure 27) where also surface features in the micro and nano scale could be seen for the laser treated implant.

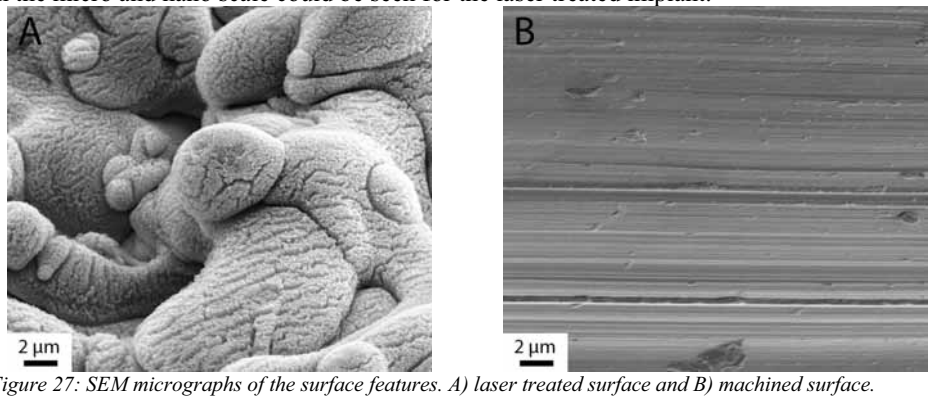

Figure 27: SEM micrographs of the surface features. A) laser treated surface and B) machined surface.

The TEM analysis in low resolution showed that the machined Ti6Al4V implant was composed of rounded grains in the subsurface. In high resolution (Figure 28A) only lattice fringes from the Ti structure are observed while the outermost layer interfacing with the protective platinum layer displays an amorphous or nano-crystalline structure. However, FFT analysis of this layer indicates that only spots representing d-spacings in the range 2.2-2.5Å exist in the image. These are most probably originating from Ti hkl planes {010}, {002} and {011}.

From low resolution TEM analysis of the laser treated sample a surface layer is seen. The surface oxide layer thickness ranges from 0.1 to 0.5µm (Figure 28C). According to the EDS analyses, the created surface layer includes, in addition to titanium and oxygen, also aluminum, one of the alloy metals. Analysis of small amounts of the other alloy metal vanadium was difficult due to that the V-Lα and Ti-Lβ lines coincide. The bulk metal had a needle form structural appearance rather than the round grains found in the subsurface of the machined sample. High resolution images of the interface between the metal and the surface layer revealed that the surface oxide is built up of crystalline grains (Figure 28B). In addition to spots in the calculated FFT originating from the structure of Ti, a spot corresponding to 2.05Å was frequently found. Obviously, it was hard to deduce the crystal structure type from one FFT spot. Since oxygen was found in the surface layer by elemental analysis, a plausible explanation is that these spots originate from one of the crystalline titanium oxides, anatase or rutile. It is however difficult to judge among the two since both have hkl d-spacings in this range. For anatase {113} the d spacing is 2.045Å while for rutile {120} the spacing is 2.054Å.

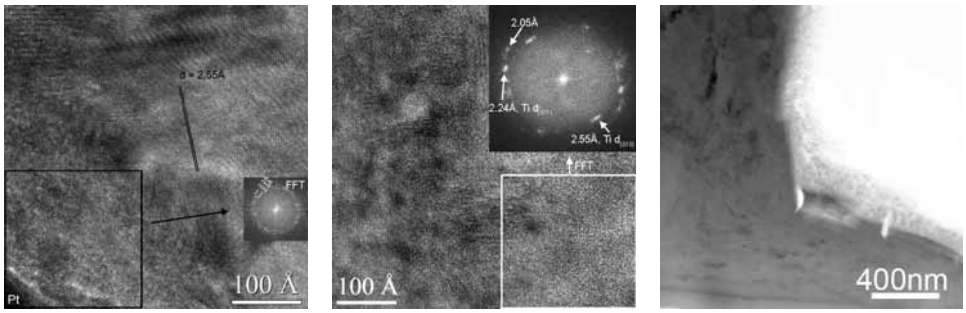

Figure 28: TEM micrographs of the implant surfaces in cross-section. A) The outermost layer of the machined implant showed an amorphous region approximately 10 nm. B) The outermost surface layer of the laser treated sample showed nano crystalline structure judged by the high resolution image and corresponding FFT. C) Low resolution image of the surface layer of the laser treated implant showing a foam like structure with nano features, ranging from 0.1–0.5 µm in thickness.

Biomechanical evaluation

The biomechanical results were unanimous and significant (p=0,005) showing that the torque at break point was on average 270 % larger for the laser treated implants compared to the machined implants (Figure 29). The maximum torque was registered at 62 Ncm (laser treated surface) while the lowest was 7 Ncm (turned surface). The mean values (with corresponding standard error) were 44,1 (3,3) Ncm for the laser treated surface and 12,6 (1,6) Ncm for the machined surface (Figure 29). The load-deformation plot showed a sharp "fracture like" break point for the laser treated implants, while the machined implants had a less well defined break point (Figure 29).

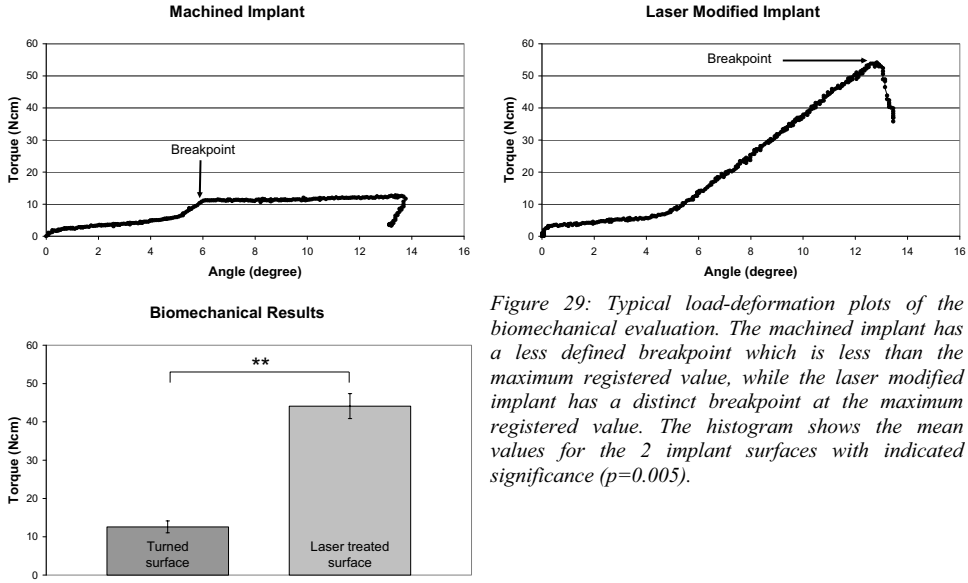

Figure 29: Typical load-deformation plots of the biomechanical evaluation. The machined implant has a less defined breakpoint which is less than the maximum registered value, while the laser modified implant has a distinct breakpoint at the maximum registered value. The histogram shows the mean values for the 2 implant surfaces with indicated significance (p=0.005).

Histology

In brief, the histological examination showed a similar general appearance as in paper IV. A main difference between the implants in paper IV and V was that the implants in paper V had been subjected to biomechanical evaluation with an applied torsional load which had

damaged the tissue-implant interface. The morphological evidence of this biomechanical test performed in anaesthetized animals prior to sacrifice, was 1) a disruption of the contact zone between implant surface and tissue (Figure 30A), 2) the presence of fracture lines in the compacta, usually located in parallel with the distinct orientation of the lamellar bone (Figure 30A), 3), the presence of a perpendicular fracture line through the mineralized bone starting at the thread top (Figure 30B), and 4) the presence of a fracture line in the bone at a distance from the implant surface (Figure 30C). The latter was exclusively detected in the bottom portion of threads with laser-modification. The finding of a disruption/fracture of the contact zone between the implant surface and the tissue precluded an accurate quantitative histomorphometric determination of the degree of implant perimeter in contact with different tissues.

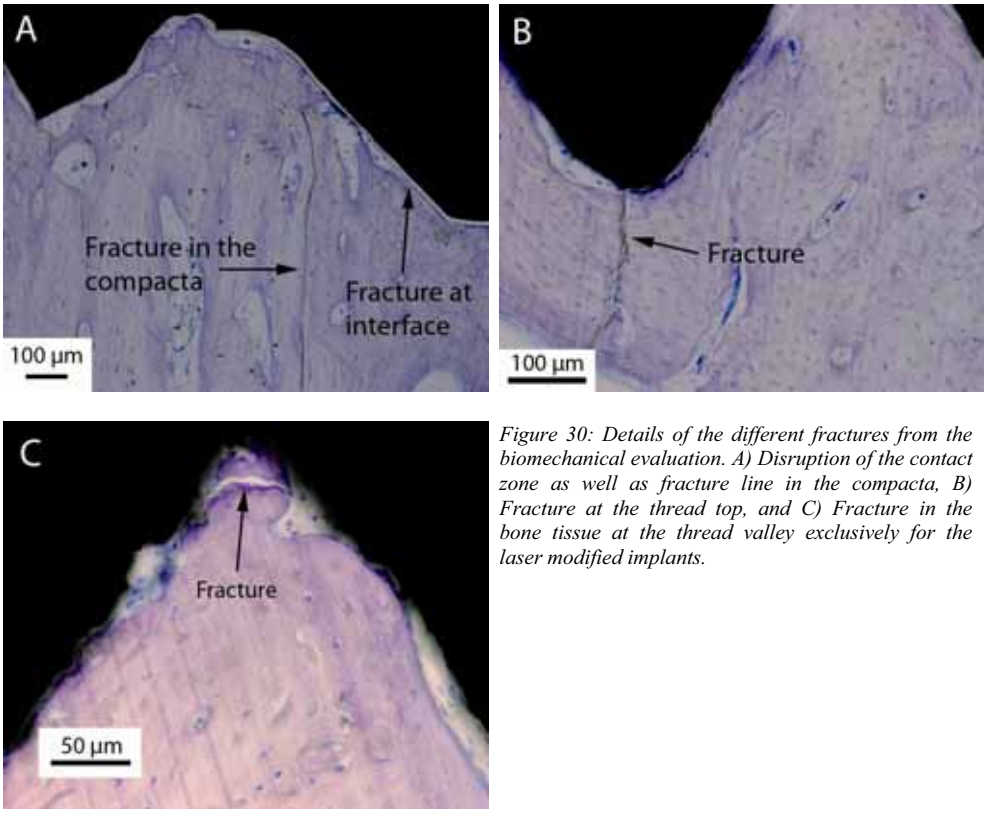

Figure 30: Details of the different fractures from the biomechanical evaluation. A) Disruption of the contact zone as well as fracture line in the compacta, B) Fracture at the thread top, and C) Fracture in the bone tissue at the thread valley exclusively for the laser modified implants.

Ultrastructure

For the machined implant no intact interface could be found according to the analysis using backscattered SEM (Figure 31A) while for the laser treated implant a large amount of bone was in direct contact with the implant at the bottom of the threads where the surface modification was applied (Figure 31B).

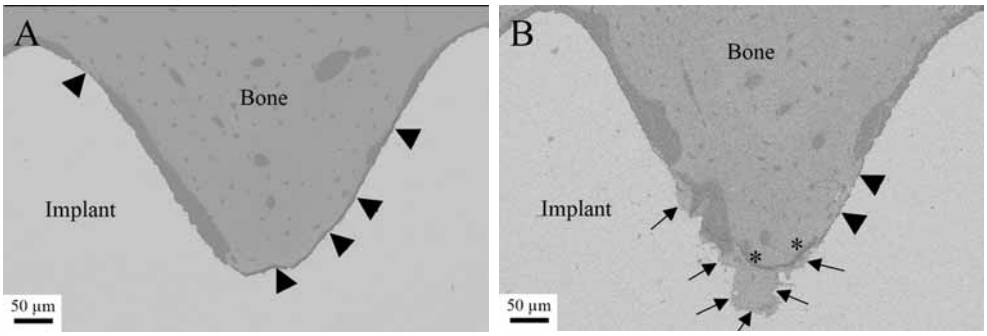

*Figure 31: Backscatter SEM images of one thread of the implant tissue bloc. A) Machined implant. B) Laser treated implant. Arrowheads points at areas with separated bone implant interface. Arrows points at areas with intact bone implant contact. * indicate the fracture line from the biomechanical evaluation.*

Trenches were cut with the FIB (Figure 32) where it could be seen that the around the machined implant the separation is found going down in the bloc following the implant surface while for the laser treated sample an intact interface was found. The laser treated implant sample was lifted out for subsequent final thinning and TEM analysis.

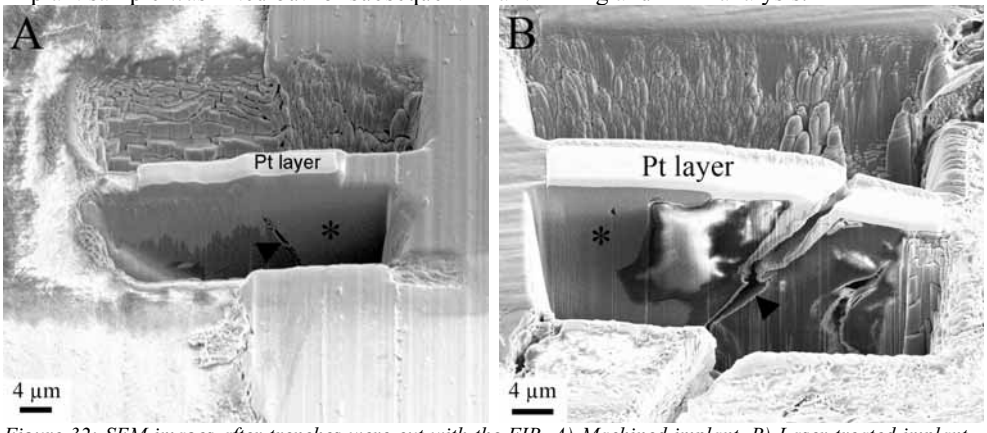

*Figure 32: SEM images after trenches were cut with the FIB. A) Machined implant. B) Laser treated implant. Implants are detected by *. Arrowhead points at the separation, however, in the case of the laser treated sample a fracture was detected in the tissue distant from the implant-tissue interface.*

The analysis of the laser treated implant-bone interface show an intimate contact at all levels of TEM resolution. The bone tissue showed the characteristic banding pattern of collagen identified close to the implant surface. No distinct border between implant and bone is observed. A coalescence of mineralized bone and the nano-textured surface is demonstrated using TEM (Figure 33). HRTEM combined with energy filtered TEM revealed the presence of calcium at the immediate implant surface.

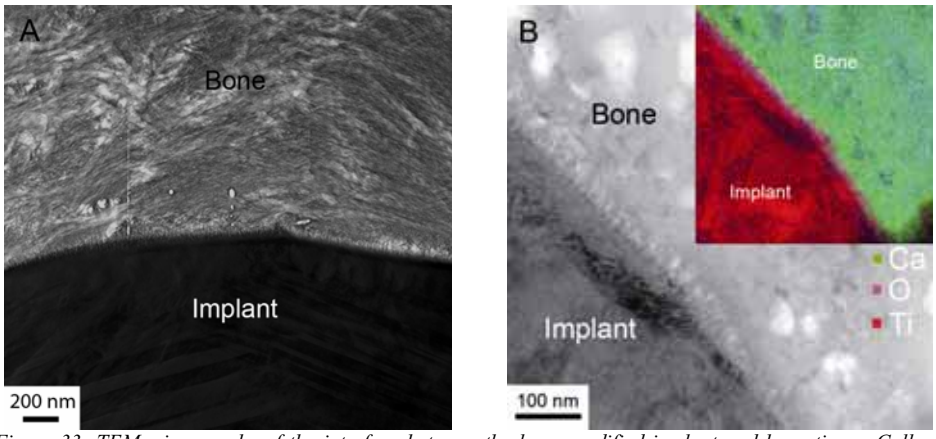

Figure 33: TEM micrographs of the interface between the laser modified implant and bone tissue. Collagen banding is seen close to the implant surface and calcium is present at the immediate implant surface, indicated by oxygen enrichment in the energy filtered insert image.

The structure of the calcium at the implant surface was identified as hydroxyapatite via high resolution TEM where the lattice fringes were recalculated to a diffraction pattern by applying fast Fourier transform. The sizes of the crystallites are in the nano range (Figure 34).

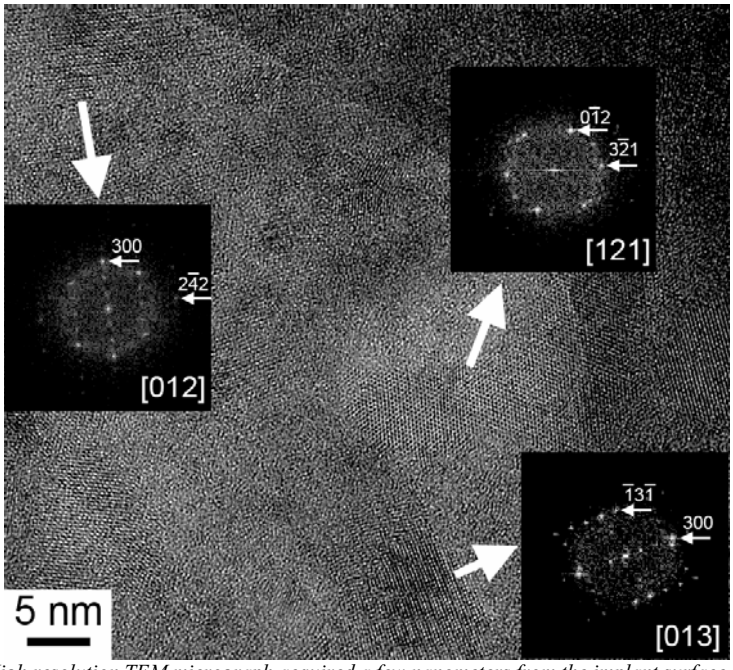

Figure 34: High resolution TEM micrograph acquired a few nanometers from the implant surface. Lattice fringes at different directions corresponding to crystallites with sizes of 5 to 20 nm, identified by FFT to be hydroxyapatite.

Discussion

Biomaterial surface analysis

Focused ion beam microscopy

The use of focused ion beam microscopy for sample preparation of ultrathin sections of the outermost layer on implants was explored in the present thesis (Paper I, II, IV and V). The thesis demonstrated a usefulness of the method, allowing cross-sections directly on the implant without prior sample preparation.
To the author's knowledge the results of focused ion beam TEM sample preparation of native oxide layers on implants have not been previously published. One publication was found using focused ion beam microscopy for sample preparation of the interface between implant bulk and hydroxyapatite coating[153]. However, the FIB has been extensively used for sample preparation of thin coatings in other applications, such as oxide layers in anodes[58], galvanized steel[154] and other surface coatings summarized in a review[90].
All methods have inherent advantages and drawbacks. It is therefore of importance that new tools are critically examined. The final role and practical implications of a new method is usually confined to future critical employment and testing by additional research groups. Nevertheless, at this stage some of the potential benefits, disadvantages and challenges may be discussed.

Important considerations which will be discussed are:

- protection of the area of interest
- possible artefacts induced by the ion beam
- limitation in sample thickness

As the surface layer often is very thin, 2-10 nm for machined implants depending on sterilization method[53], different techniques for protection were evaluated (Figure 35). By using platinum deposition by ion assisted chemical vapor deposition directly at the surface it was shown that the thin native oxide on machined implants could be etched and destroyed (Paper I). By applying a thin electron assisted deposition prior to the ion assisted deposition, the surface oxide was protected and still present. It has previously been suggested that protection by a thin layer of chromium [155] or gold sputter coating[58,156] could be used prior to mounting the sample in the FIB. We have also used plastic embedding of the implant prior to sectioning samples with the FIB (Paper IV and V) where the surface layer of interest is not directly striked by the ion beam (Figure 35).

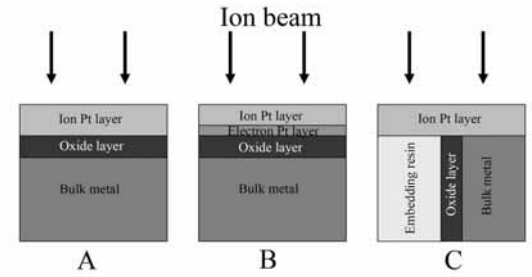

Figure 35: Schematic image of the different techniques for protecting the area of interest. A) Only by ion assisted Pt deposition. B) Electron followed by ion assisted Pt deposition. C) Embedding in resin prior to FIB preparation.

The plastic embedding is frequently used in the conventional TEM preparation in the material science field, where often two surfaces are glued together and ground, polished and ion milled (argon ions) to electron transparency prior to TEM analysis. For implant surfaces, only one article has been found using the conventional preparation technique[55] and was not applied on screw shaped implants but rather on titanium disks prepared by similar surface treatment as the implant. For thinner oxide layers, as the machined surface (~10 nm) the plastic resin could be interfering with high-end TEM analysis, due to the presence of oxygen and the amorphous structure, especially for thicker samples as the FIB produced (~100 nm).
Other limitations with the FIB is the limited size of the sample, where the normal size is 30x10 µm[96] however, larger sample could be made with sizes up to hundreds of microns[157] but much more time consuming.
Also different lift-out methods have been evaluated during the work where *in situ* and *ex situ* were employed as sample preparation for surface analysis (Paper I, II, IV and V). The disadvantage of the *in situ* lift out method is that it is more time consuming and also more operator dependent using the micromanipulator and soldering to the TEM grid. However, the advantages are numerous with improved sample quality, possibility to additional thinning of the sample if needed and no intervening carbon coating on the grid. Further, the results from the thesis show that a higher sample yield is obtained by the *in situ* lift-out method (Paper I). We have suffered lost sample due to repulsion forces to the glass needle when using the *ex situ* lift-out method, something which might be possible to improve. Other disadvantages for the *ex situ* method are limited depth of focus for highly irregular samples, and difficulties in reaching the sample with the glass needle[154]. Further, by tilting the sample during final thinning a wedge like structure could be obtained where the thickness gradually decreases either from the top or the bottom[158]. Depending on the pre-preparation of the specimen benefits could be obtained by extra tilting during the final thinning, where an embedded sample would always be found at the along the gradient whereas samples taken directly from the implant surface would not benefit from this preparation(Figure 36).

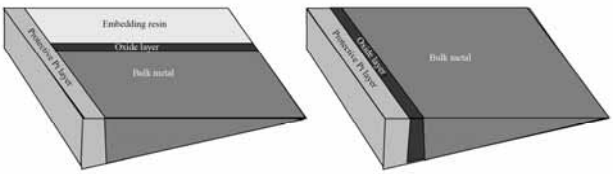

Figure 36: Schematic image of FIB prepared samples obtained directly at the surface (right) or after plastic embedding (left). In order to make very thin samples tilting during final thinning is possible. With plastic embedded sample the area of interest is always present at different thicknesses while the sample taken directly from the surface shows differences in thickness from the bulk metal.

Other technical difficulties during the FIB sample preparation may cause the so-called amorphization and redeposition artefacts. The redeposition is mainly a problem when using the *ex situ* lift-out technique where the whole sample is prepared in the trenches and material could sputter back on the sample, but by using the low beam current at the final steps of thinning this is minimized[92]. The amorphization has been shown to be around 10 nm using 1000 pA ion beam on silicon[92] and less when using lower beam currents at the final thinning[159]. As preparation of samples thinner than 50 nm is very difficult and the normal sample thickness is around 100 nm[155] the affected zone is only a fraction of the sample and would therefore not be a major interference of the subsequent analysis.
The different FIB methods used in the thesis for sample preparation have shown advantages and disadvantages. The *ex situ* lift-out technique was faster (2-3 hours) compared to the *in situ* lift out technique (5-7 hours), however, the subsequent TEM analysis of the ex situ produced sample will have an interfering carbon coating on the TEM grid[96] while only the sample is in the electron beam path for the *in situ* prepared sample.

Implant surface analysis

Modifications of implant surfaces are introduced clinically with regular intervals. Whether such surface modifications infer significant paradigm shifts or incremental step-wise improvements in clinical performance is not known. According to evidence-based, Chochrane Systematic Reviews, small or no differences in clinical performance were found when reviewing the literature for randomized clinical trails of different implant systems[160-164]. Surface modifications belong to either chemical or topographical alterations. Much attention has been focused on the modification of surface texture. Of particular interest is that such alterations are usually resulting also in changes of the chemistry[165]. The non-intentional changes of other surface parameters have to be determined and their role determined. On this background it is imperative to fully characterize the combination of chemical and topographical surface properties of implants which are used clinically. The present studies demonstrated that the combination of FIB and TEM provides new, hitherto unpublished data on the properties of clinically used oral implant surfaces in contact with the biological system. Important characteristics of the surface are oxide thickness, morphology and phase composition. This is a field which has been largely unexplored for dental and orthopaedic implants, where the main focus has been on the bonding energies and thickness of the oxide layer[52,53,166]. However, it has been suggested that the different phases of TiO2 might have an effect on the *in vivo* performance. The Kukobo *in vitro* bioactivity test[167] has been performed on a variety of titanium surfaces with different compositions of rutile and anatase[168-170] and it has been found that the apatite formation occurs differently at the different crystal directions[171]. Therefore new techniques enabling analysis of the phase composition is required.
With the FIB sample preparation for TEM analysis the present studies demonstrated large differences in the morphology and phase composition between different commercially available implants and test implants (Table 7). Regrettably, for the SLA surface we could not resolve the surface layer due to difficulties in sample preparation caused by uneven Pt deposition on the highly irregular and sharp surface features. The SLA surface has been suggested to be an amorphous titanium oxide with a subsurface of titanium hydride[55,172,173]. In contrast to previous suggestions of an incorporation of fluoride in the oxide layer[174], the OsseoSpeed surface was found to possess a dual surface layer, with different oxide thicknesses and crystallinity, where fluoride could be detected by XPS but not with TEM indicating a monolayer of fluoride on the immediate surface. For the TiUnite surface we found a mixture of amorphous and anatase containing surface with no rutile which

has been found earlier[175] which most likely is due to the limited area analyzed in the present thesis. However, it cannot be excluded that also the fabrication process plays a role, since it has been changed since the latter reference was published. Further, the outermost layer was always amorphous in our samples, potentially important information which could not be detected by other phase analysis as XRD and Raman.

The original surface showed some crystalline (rutile) and some amorphous areas. Other TEM analyses of such surfaces have shown that with heat treatments above 250°C, the surface layer starts to crystallize[57]. For Ti6Al4V similar studies have shown that the crystallization temperature is about 400°C[56]. The machining process might generate temperature locally exceeding the crystallization temperature which renders some areas crystalline while others are amorphous. The present studies demonstrated an amorphous structure of the oxide layer for the machined Ti6Al4V implants, while the laser modified Ti6Al4V surface was crystalline. The laser process will melt the surface material at high temperature which will be splashed around and rapidly cooled down, this process seems to generate both a phase shift in the subsurface[176] as well as crystallization of the oxide layer.

The present results regarding the biomaterial surface analysis have shown that the commercially available implants and test implants all possess differences in both surface topography and elemental and phase composition of the oxide layer. It has earlier been strongly suggested that the surface topography plays a role in the biological response to implants[33,34,177]. Implants have been categorized according to the magnitude of the topography and it has been suggested that the moderately rough implants have an improved bone response compared to the other categories[32]. However, the surface topography is not completely straight forward and a variety of values of different parameters have been reported for different commercially implant surfaces[174,175,178-180]. To sort this out guidelines have been suggested for the measurements[181]. The present surface topographical analysis using interference microscopy shows similar values as previously reported for SLA, OsseoSpeed, HA coated and TiUnite. In contrast, large differences was found for the machined implants between different sizes of analyzed areas (Table 7) comparing the results for paper II and paper IV where similar surfaces have been analyzed. Both values are outside the reported values in literature where it has been found to be between 0.3 to 1.0 for machined surface using different techniques and probably different sizes of analyzed areas[50]. One possibility to this difference is the size of analyzed area as well as the filtering and mathematical corrections of the raw data obtained by the instrument. Some filters may underestimate the surface topography by filter away larger scratches, while these might not even be included in the area of analysis when choosing a smaller area of analysis. Further, the machining process (turning speed and the material of the tools) and lubricant used might influence the surface topography.

Further, regarding the isotropic features of the surfaces, it was found that the machined and laser modified implants have an anisotropic topography with preferential direction along the machining and laser direction. The role of this phenomena is not completely understood but it may influence the cell alignment along micro and nano fabricated surfaces[182,183]. Further, by applying a micron (100-200 μm) sized groove following the threads on the implant surface, higher bone implant contact has been found[184].

	Commercial implants					*Test implants*		
Surface name	**SLA**	**Osseospeed**		**Hydroxyapatite coated**	**TiUnite**	**Original**	**Machined Ti6Al4V**	**Laser modified Ti6Al4V**	
Surface modification	Blasted and dual acid etched	Blasted and acid etched, diluted HF		Plasma sprayed	Anodic oxidation	Machined	Machined	Machined and laser modified in the valleys of the threads	
								Machined	Laser modified
Roughness Large area* Small area**	1.98	1.82		3.29	1.55	1.53 0.33	- 0.30		- -
Direction	Isotropic	Isotropic		Isotropic	Isotropic	Anisotropic	Anisotropic		Anisotropic
Surface features	Sharp edges	Semi sharp edges		Smooth round edges	Smooth round edges	Semi sharp edges	Semi sharp edges		Smooth edges
Surface structure	Homogenous	Inhomogenous		Homogenous	Homogenous	Homogenous	Homogenous	Inhomogenous	
		Islands	Lower surface					Machined	Laser modified
Oxide thickness TEM AES	- -	0.5-1 µm -	10 nm -	> 5 µm -	2 µm -	10 nm 5 nm	10 nm 5 nm		0.1-0.5 µm 390 nm
Bulk-oxide interface	-	Porous		-	Porous				
Oxide bulk	-	Crystalline, rutile and anatase	Amorphous	Crystalline, hydroxyapatite	Amorphous and crystalline, anatase	Amorphous and crystalline, rutile	Amorphous		Nanocrystalline, phase unidentified
Elements in the oxide	-	Fluoride***-		Calcium and phosphorous	Phosphorous		Aluminum and vanadium		Aluminum and vanadium
Immediate surface	-	Partly crystalline		Amorphous	Amorphous	Partly crystalline	Amorphous	Partly nanocrystalline	

*Table 7: Summary of the surface analyses performed on the different implants, both commercially available and test implants used in the thesis. *roughness measurements performed according to paper II, ** roughness measurements performed according to paper IV. *** according to XPS analysis.*

Bio-interface analysis

Biomechanics and histology

In paper III we have shown that a machined c.p. titanium implant was osseointegrated after 11 years in human with large amount of bone around as well as in direct contact with the implant judged by light optical microscopy (75 and 85 % respectively). A high degree of osseointegration has earlier been demonstrated for dental implants[30] and craniofacial implants retrieved for human[185] while non-cemented metal arthroplasties are often associated either with a fibrous membrane or limited bone ingrowth/bone-implant contact[24-26]. Further, for dental implants which had been in functional load, a higher bone-implant contact was found compared to un-loaded implants retrieved implant[186]. The implant which had been in functional loading during most of the time in situ had fractured caused by fatigue. By using implants materials with improved mechanical properties such problems may be limited for high load bearing implants such as the bone anchored amputation prostheses.
Ti6Al4V has higher yield strength and resistance to fatigue compared to c.p. titanium[187-189]. The present results did not reveal any differences in bone response to machined c.p. titanium and Ti6Al4V after 8 weeks of healing in rabbit tibia (Paper IV). The bone reactions toward differences in implant materials have been extensively studied especially the reactions around c.p. titanium and Ti6Al4V. However, the results are not conclusive whether there are any differences in the bone response. Many studies have shown no differences in histomorphological evaluations between the materials with similar surface structure[64,112-114,190] while some studies have shown less mineralization in the interfacial tissue toward the implant surface of Ti6Al4V compared to c.p. titanium on the light optical level[115,130]. Small differences were found in the attachment to the bone as evaluated by biomechanical testing by torsion[64,112,114,191]. On the ultrastructural level, either using titanium and Ti6Al4V sputter coated plastic plugs or using real bulk metal implants with subsequent fracture technique for TEM sample preparation, the interface to Ti6Al4V in comparison to c.p. titanium has been differently described. A larger amorphous zone containing proteoglycans and glycosaminoglycans have been reported in contact to Ti6Al4V[130] while no differences in the interface was found with the bulk implants[136]. Concerns regarding ion leakage has been reported and discussed for titanium and titanium alloy implants[115,192] and *in vitro* corrosion studies have been performed for evaluating the re-passivation occurring in simulated biological environment[193]. Further, it has been shown that wear is an important factor for the ion leakage while the surface roughness and specific surface area was less important[192,194]. However, the clinical effect of ion leakage seems limited since long term success have been reported for both orthopaedic and dental implants[20,31,195].

By modifying parts of the implant surface (thread valleys) with laser, creating micro and nano features, the biomechanical properties of the bone anchored implants were increased with 270 % compared to machined implants (Paper V). Similar increase in the biomechanical anchorage has been found for laser modified implants of c.p. titanium[40,196,197]. No qualitative difference was found in the bone response between partly laser modified machined implant and machined implant as judged by light optical histology after 8 weeks of healing while higher bone-implant contact has previous been found for c.p. titanium implants with similar laser treatment in the valleys of the threads[196,197]. The clinical possibilities of implants with both increased intrinsic mechanical properties and increased biomechanical anchorage in bone are numerous, where higher load could be applied. The size of the implant could be reduced as well as the patient criterion could be extended. Further, by keeping the majority of machined implant unchanged, possibly lower frequency of peri-implantitis may be expected[198].

Focused ion beam microscopy

Focused ion beam milling for TEM sample preparation of interfaces between bone and implant materials is largely unexplored in the literature. Five papers concern the bone implant interface[79,105-107,199]. Two papers demonstrate the absence of an intact interface between bone and a failed titanium implant but the reason for the observation (due to the preparation steps and or the properties of the implant or host) is difficult to judge since essential details such as fixation, dehydration and stabilization) prior to sectioning with the FIB were not provided[106,107]. The other publications concerns hydroxyapatite and zirconia scaffolds[105], hydroxyapatite coated titanium implant[79] and calcium aluminate coated cobalt chromium implant[199].

The thesis presents for the first time TEM analysis of the intact interface between bone and both clinically retrieved high loaded amputation prosthesis and laser modified Ti6Al4V implants. The FIB preparation of such interfaces showed limited preferential milling of the softer part (bone) compared to the implant material, on the contrary to the ultramicrotome cutting, where cutting of both materials is not possible except of getting small residuals of implant material in the section[21]. The FIB produced samples were of such quality enabling high resolution analysis as well as energy filtered analysis giving new insight of the osseointegration process to titanium implants.

The results of the present thesis show difficulties of obtaining intact interfaces depending on the bone bonding ability of the material where important features are surface topography and surface chemistry. The pre-FIB treatment of the specimen is most likely important for the possible outcome with FIB milling of electron transparent sections of the intact interface. It has been shown that the fixation as well as the dehydration affect the volume of the retrieved tissues[200]. Further, it has been suggested that the embedding resins might have an effect as well. The present results indicated that the importance of the embedding resin was less than the bone bonding ability to the implant surface (Paper IV). Hence, for relatively smooth implants as the machined implant, separation is a cumbersome problem for FIB sample preparation but on the other hand these results indicated the usefulness of the fracture technique for cases where limited bone bonding has occurred. On the other hand, by adding a thin coating of hydroxyapatite (100 nm) the bone bonding properties of the implant becomes enough to withstand the shrinkage of the tissue during fixation, dehydration and embedding[79]. The effect of surface topography has been shown to increase the biomechanical strength of the interfacial bond between implant and tissue[33,40,177]. This might create sufficient mechanical interlocking of the tissue to withstand the shrinkage of the tissue without disruption of the interface zone as observed in paper V. Also the healing time and loading conditions might have an impact in the bonding properties to a machined implant. This was suggested for the amputation prosthesis retrieved after 11 years of healing, where most of the time used with functional loading, allowed a semi intact interface for sectioning with the FIB (paper III). Other limitation with the FIB for TEM sample preparation of tissue-implant interfaces compared to the conventional ultramicrotome sectioning is the sample size. With the FIB only a very limited sample (30x10 μm) could be sectioned, where at a distance from the implant were few cells are present. Further, the size of the cells is generally larger than the FIB sectioned sample. An advantage with the ultramicrotome is that when the specimen is prepared for sectioning, either by using metal coated plastic plugs, bulk metal dissolved by electrochemical process or the implant is removed and the actual interface is located, rather rapid serial sectioning is possible. For the FIB the localization of the interface is rapid but each sample takes a few hours of work. However, the intact interface with both the tissue and implant present is possible in contrast to the conventional ultramicrotome. Only one publication has been found sectioning the intact interface between implant and tissue using the ultramicrotome at an oblique angle obtaining only a fraction of the implant in the

section[21]. As the FIB sectioning was performed on resin embedded specimen the ultrastructural analysis could be performed in combination with histological analysis of the same implant and no special treatment was needed.

Ultrastructural analysis

The chemical and molecular composition of the interfacial tissue is a key issue for further understanding of the osseointegration process. Different theories have been forwarded and discussed, from the point that the interface is composed of an almost unmineralized ground substance[76] to a fully mineralized cement line appearance in the immediate interface[201]. Further, the nomenclature of the interposed layers in the interface varies with authors and publications. Here, the layer termed **electron lucent** has been referred to ground substance layer and amorphous layer, briefly a layer consisting of non mineralized or sparsely mineralized layer without fibrillar structure. The term **electron dense layer** has also been referred to amorphous layer by some authors, briefly a mineralized afibrillar layer. Both these layers have been found to consist of proteglycans and glycosaminoglycans according to ruthenium red and lanthanum contrasting[76,120], however a difference was found regarding ostecalcin and osteopontin, where the latter was found in the electron dense layer while the former was found in the electron lucent layer[134]. The different interfaces found for titanium implants are summarized (Figure 37). The present results show some difference in interface composition between the c.p. titanium implant and the Ti6Al4V implant, where both show apatite at the immediate implant surface. For the functionally loaded machined c.p. titanium implant retrieved from human (Paper III) an apatite layer was demonstrated followed by an electron dense zone consisting of tightly packed hydroxyapatite crystals prior to the bone tissue with the characteristic collagen banding (Interface H, Figure 37). For the micro- and nano-structured Ti6Al4V (Paper V) mineralized tissue was demonstrated at the immediate interface as judged by the presence of collagen banding and HRTEM of apatite structure (Interface B, Figure 37). Cement lines were not detected but since the samples were undecalcified and rather thick (100 nm) compared to ultramicrotome prepared sections (40-70 nm) the presence of a cement line at the immediate interface cannot be excluded.

The clinical effect of the different interfaces is difficult to judge, and most of the interfaces most likely co-exist within different areas around the implant. Only one author has performed serial sectioning of the complete bone adjacent to the implant and it was reported that the bone tissue differs at areas of resorption and remodeling, and areas with less mature bone (interfaces E and F, Figure 37)[119]. Further, different microscopic techniques, contrasts, healing and loading conditions may influence the analysis as well as the acceleration voltage of the microscope. Most of the studies found in the literature have used microscopes designed for biological analysis and often limited to rather low acceleration voltages. Some of the references have stated the acceleration voltage during analysis, where most used was between 60-100 kV[8,82,83,119,120,122-126,133] and a few using 200 kV[79,106,107,147,148], while in the present thesis acceleration voltages of 200-300 kV has been used, enabling higher resolution and analysis of thicker samples. The present results showed differences for similar implants with different healing times, loading conditions and species(paper III and IV) where it was impossible to prepare intact samples of the latter (non-loaded; short healing time). According to Steflik et al, no difference was observed in the interface zone for different materials chemistry (titanium vs ceramic) or loading (non-loaded vs functional loading) on the ultrastructural level while differences were observed at the light optical level[120]. In the present thesis, an intact fully mineralized interface could be analyzed when a micro- and nano-featured surface was created by laser, showing a perfect congruency of mineralized bone and implant surface in high resolution TEM.

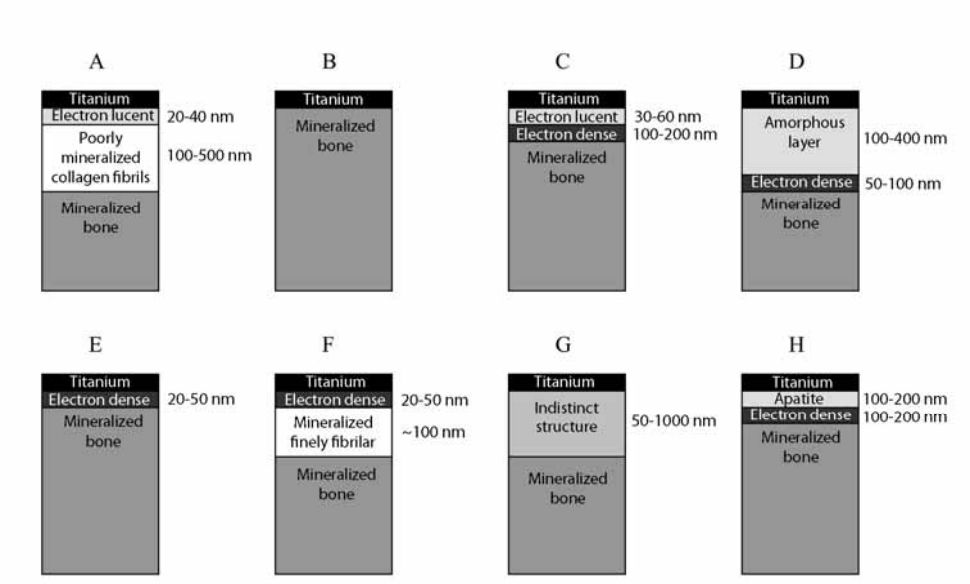

Figure 37: Schematic images of the typical titanium-bone interfaces found in literature and during the thesis work A) Typical interface found by many authors[76,77,81,83,106,107,127,128,130,131,134,135,142,143] where most of the authors have used decalcified specimen, however some with un-decalcified specimen, using different sample preparation techniques, plastic plug, fracture technique and FIB. Further different species and healing times have been reported. B) Mineralized bone in direct contact with the implant surface have been reported in the literature[21,79,117,118,141,144,147,148] and also found by us with laser modified Ti6Al4V. Different sample preparation has been reported, such as direct ultramicrotome cutting without prior removal of the implant, plastic plug, fracture technique and FIB.. All authors have used un-decalcified specimens from a variety of species including human, dog, rabbit and rat. C) An interface composed of 2 intervening layers, electron lucent followed by electron dense have only been reported for decalcified specimen using the plastic plug method[133] while the same research group found a similar interface with reversed layers in another publication[68] using the same preparation method. D) An interface found using fracture technique[132,145] and a combination with electropolishing[30,84,116] for implants retrieved from rabbit and human. All specimens were un-decalcified prior to sectioning. The amorphous layer was reported to be afibrillar without any structure and could not be excluded to be an artefact, possibly from the embedding with LR White (compare Paper III). E) A mineralized electron dense layer interposed between implant surface and bone has been reported and discussed as a cement line like structure using the fracture technique on specimens both loaded and non-loaded from dog[8,82,119-126] and from rat[81,134]. F) Similar interface as E found at areas where the bone was undergoing remodeling or was less mature[8,82,119-126,142]. G) An indistinct interfacial interposed layer have been reported consisting of fibrillar, non-fibrillar or granular structure from both decalcified and undecalcified sections from rabbit and human[136,147,148] H) Results from the present thesis with crystalline apatite formation directly at the implant surface after 11 years of clinical use (Paper III). Detailed descriptions of the sample preparation methods and analytical techniques used for corresponding interface are found in Table 1, 2 and 3 in the introduction.

For future studies, more interfaces should be studied, linking the surface structure to its interface to bone, for further understanding the relevance of the phase composition of the implant surface (amorphous, rutile and anatase) and the bone formation in both experimental and clinical trials. Further, to evaluate the possibilities for immunocytochemical contrasting of biomolecules by colloidal gold particles of FIB prepared intact interfaces between implant material and tissue is an interesting future challenge.

Summary and Conclusions

- An *in situ* lift-out technique for FIB preparation of TEM samples showed higher yield and sample quality compared to an *ex situ* lift-out method. Further, protection of the surface by a thin coating of electron assisted platinum deposition prior to ion assisted platinum deposition was essential in order to avoid surface damaging by the gallium ion bombardment.

- The preparation by FIB of TEM samples in cross-section provided new possibilities to characterize the outermost surface layers of differently modified, clinically used oral implants, in particular, the morphology and phase composition. Limitations were observed for highly irregular and sharp surface structures.

- The FIB preparation of ultrathin sections of the intact bone-implant interface combined with light optical histology provided for the first time a correlation between a mineralized bone interface and the clinical function of bone anchored amputation prosthesis.

- Embedding resins frequently used for histology revealed large differences with respect to bonding to machined c.p. titanium implants.

- A similar bone response was detected for machined c.p. titanium and Ti6Al4V implants after 8 weeks of healing in rabbit tibia, as judged by histology and histomorphometry. A limitations regarding FIB sample preparation was observed for specimens which did not provide sufficient bonding (mechanically or chemically) to the implant surface.

- FIB sample preparation with subsequent TEM analysis could effectively be used in combination with biomechanical evaluation and histology in a study of laser modified and machined Ti6Al4V implants after 8 weeks in rabbit tibia. The study demonstrated a 270% increase in torque value, a different fracture pattern and a direct contact between nanocrystalline hydroxyapatite and the oxide surface. Taken together, these observations suggest, firstly, a stronger bone-implant interface for laser modified surfaces in comparison with machined implants, and, secondly, a correlation between the ultrastructure (down to the Ångström level) of the intact interface and its biomechanical properties.

In conclusion, the results of the present thesis demonstrate that FIB is a new and promising preparation technique enabling high resolution analysis of both native implant surfaces and their interfaces to bone. Taken together, the present observations suggest that FIB in combination with TEM provide important ultrastructural information, complementary to available surface analytical, histological and biomechanical tools for the evaluation of biomaterials.

Acknowledgements

This thesis was made in cooperation with the department of Biomaterials and department of Orthopaedics at Sahlgrenska Academy at University of Gothenburg, Göteborg, Sweden; the department of Material Science at Ångström Laboratory, Uppsala University, Uppsala, Sweden and the Institute of Biomaterials and Cell Therapy (IBCT), Göteborg, Sweden.

I would like to express my deepest gratitude to all colleagues and friends who have been directly or indirectly involved in the work with this thesis, in particular:

Professor Peter Thomsen, my supervisor, for giving me the opportunity to fulfill this thesis work, your supervision, your ability to see new possibilities and your curiosity and guidance throughout the work.

My co-supervisors, Rickard Brånemark, department of Orthopaedics, Håkan Engqvist, department of Material Science and Tobias Jarmar, Doxa AB, for your great knowledge in the different disciplinary and for all your support and patience.

Lena Emanuelsson and Anna Johansson, department of Biomaterials, for your skillful work with biological specimen preparation and analysis and for all interesting discussions.

Fredrik Lindberg, department of Materials Science, for your engaged work with electron microscopy.

Staffan Sjödin, IBCT, for much of the administrative work and general guidance through my work.

Fredrik Ericsson, MSL, Uppsala University, for your guidance and support during my microscopy sessions.

The colleagues at the department of Biomaterials, especially Barbro Lanner, for support during administrative procedures, Professors, Thomas and Lars for sharing your personal opinions of bone-implant interface. Maria for your software support. And all the PhD students, Sofia, Omar, Sara, Byung-Soo, Giusseppe, Amir, Costas and Viktoria, keep up the good work.

All colleagues at Integrum AB, Göteborg, in particular Thomas and Carl for your knowledge regarding implant manufacturing and design.

All colleagues at the department of Material Science, Uppsala University.

All the people at GöteborgBio for providing a nice biomaterial environment in Göteborg.

I would also like to thank my family and all my friends not directly involved in my work **for making life wonderful**, especially

Oskar Westin for making my life great outside the Ångström Laboratory, Uppsala

Andreas Stepien, for great mentoring during Monday dinners at the best restaurants in Göteborg.

Henrik, Aase and Micke, Frida and Björn, Frida and Mats, Christian and Emma for reminding me of a life outside work.

For spiritual support, my late mother, Kerstina. My father Krister for always being supportive and showing me around the wide world. My brother Mikael and my sister Eva, with families, for guidance and love.

And finally, Sara for your love, support and patience.

Since the start of my PhD studies in January 2006, different parts of my studies have been funded by the following grants:

VINNOVA VinnVäxt Program Biomedical Development in Western Sweden (Institute of Biomaterials and Cell Therapy, IBCT, together with Integrum AB and Doxa AB) (providing me with an excellent innovation environment with Project Beta: development of the FIB/TEM technique for implant surfaces and implant-bone interfaces) (www.goteborgbio.se)

Swedish Research Council (grant K2006-73X-09495-16-3) (The interface between biomaterials and tissue) (providing me with the basic science tools for exploring the interface)

VINNOVA Forska&Väx (2006-02247) (provided to Integrum AB for verification of new surface modification and Ti alloy materials)

VINNOVA VinnBay Program (providing me the opportunity to spend a 3-month period in 2006 in the R&I environments of Professor Stuart B. Goodman, Department of Orthopaedic Surgery, Associate Professor Rainer Fasching and Professor Fritz B. Prinz, Rapid Prototyping Laboratory, Stanford University, USA)

VINNOVA VinnExcellence Center of Biomaterials and Cell Therapy (BIOMATCELL) (providing me with an excellent environment and possibilities for meetings and interactions with people from different fields: academia, health care and industry (www.biomatcell.se)

Region Västra Götaland and LUA/ALF Göteborg grant (Optimization of osseointegration for treatment of amputees), (www.fou.nu/is/sverige/document/5291)

Other personal funding for increasing my quality of life and travel expenses was received from Stiftelsen Markussens Studiefond 2008 (www.markussens.se) and Erik och Majken Wagnstedts Resebidrag

References

[1] Weiner S, Arad T, Traub W: Crystal organization in rat bone lamellae. FEBS Lett 1991; 285:49-54.

[2] Cowin SC: Bone poroelasticity. J Biomech 1999; 32:217-238.

[3] Proubasta I, Mur JG, Planell JA, Vazquez JJ: *Fundamentos de Biomecánica y Biomateriales*. Madrid: Ergon, 1997, p. 377.

[4] Doblaré M, García JM, Gómez MJ: Modelling bone tissue fracture and healing: A review. Engineering Fracture Mechanics 2004; 71:1809-1840.

[5] Brånemark R: *A Biomechanical Study of Osseointegration: In-vivo measurements in rat, rabbit, dog and man*. Department of Orthopaedics. Göteborg: Göteborg University, 1996, pp. 106.

[6] Lanyon LE: Osteocytes, strain detection, bone modeling and remodeling. Calcif Tissue Int 1993; 53 Suppl 1:S102-106; discussion S106-107.

[7] McKee MD, Farach-Carson MC, Butler WT, Hauschka PV, Nanci A: Ultrastructural immunolocalization of noncollagenous (osteopontin and osteocalcin) and plasma (albumin and alpha 2HS-glycoprotein) proteins in rat bone. J Bone Miner Res 1993; 8:485-496.

[8] Steflik DE, Sisk AL, Parr GR, Lake FT, Hanes PJ, Berkery DJ, Brewer P: Transmission electron and high-voltage electron microscopy of osteocyte cellular processes extending to the dental implant surface. J Biomed Mater Res 1994; 28:1095-1107.

[9] Ginebra MP: *Desarrollo y caracterización de un cemento óseo basado en fosfato tricálcico-A para aplicaciones quirúrgicas*. Departament de Ciència dels Materials i Enginyeria Metallúrgica Barcelona: Universitat Politècnica de Catalunya, 1997, pp.

[10] Miller A: Collagen: the organic matrix of bone. Philos Trans R Soc Lond B Biol Sci 1984; 304:455-477.

[11] Stevens MM, George JH: Exploring and engineering the cell surface interface. Science 2005; 310:1135-1138.

[12] Weiner S, Traub W: Bone structure: from angstroms to microns. FASEB J 1992; 6:879-885.

[13] Weiner S, Traub W: Organization of hydroxyapatite crystals within collagen fibrils. FEBS Lett 1986; 206:262-266.

[14] Davies JE: Understanding peri-implant endosseous healing. J Dent Educ 2003; 67:932-949.

[15] Davies JE, Nagai N, Takeshita N, Smith DC: *Deposition of cement-like matrix on implant materials*. In Davies JE, ed: The bone-biomaterial interface. Toronto: Univ. of Toronto Press, 1991, pp. 502 s.

[16] Puleo DA, Nanci A: Understanding and controlling the bone-implant interface. Biomaterials 1999; 20:2311-2321.

[17] Szmukler-Moncler S, Salama H, Reingewirtz Y, Dubruille JH: Timing of loading and effect of micromotion on bone-dental implant interface: review of experimental literature. J Biomed Mater Res 1998; 43:192-203.

[18] Carter DR, Giori NJ: *Effect of mechanical stress on tissue differentiation in the bony implant bed*. In Davies JE, ed: The bone-biomaterial interface. Toronto: Univ. of Toronto Press, 1991, pp. 502 s.

[19] Frost H, Joos U, Meyer U, Jensen OT: *Dental alveolar distraction osteogenesis and the Utah paradigm*. In Jensen OT, ed: Alveolar distraction osteogenesis. Chicago: Quintessence Pub. Co., 2002, pp. xi, 187 s.

[20] Brånemark PI, Hansson BO, Adell R, Breine U, Lindstrom J, Hallen O, Ohman A: Osseointegrated implants in the treatment of the edentulous jaw. Experience from a 10-year period. Scand J Plast Reconstr Surg Suppl 1977; 16:1-132.

[21] Albrektsson T, Branemark PI, Hansson HA, Lindstrom J: Osseointegrated titanium implants. Requirements for ensuring a long-lasting, direct bone-to-implant anchorage in man. Acta Orthop Scand 1981; 52:155-170.

[22] Brånemark PI: *Introduction to osseointegration*. In Brånemark P-I, Zarb GA, Albrektsson T, eds: Tissue-integrated prostheses : osseointegration in clinical dentistry. Chicago: Quintessence Publ. Co. Inc., 1985, pp. 350 s.

[23] Morshed S, Bozic KJ, Ries MD, Malchau H, Colford JM, Jr.: Comparison of cemented and uncemented fixation in total hip replacement: a meta-analysis. Acta Orthop 2007; 78:315-326.

[24] Bloebaum RD, Mihalopoulus NL, Jensen JW, Dorr LD: Postmortem analysis of bone growth into porous-coated acetabular components. J Bone Joint Surg Am 1997; 79:1013-1022.

[25] Cook SD, Thomas KA, Haddad RJ, Jr.: Histologic analysis of retrieved human porous-coated total joint components. Clin Orthop Relat Res 1988:90-101.

[26] Fornasier V, Wright J, Seligman J: The histomorphologic and morphometric study of asymptomatic hip arthroplasty. A postmortem study. Clin Orthop Relat Res 1991:272-282.

[27] Lester DK, Campbell P, Ehya A, Rude RK: Assessment of press-fit hip femoral components retrieved at autopsy. Orthopedics 1998; 21:27-33.

[28] Bauer TW, Geesink RC, Zimmerman R, McMahon JT: Hydroxyapatite-coated femoral stems. Histological analysis of components retrieved at autopsy. J Bone Joint Surg Am 1991; 73:1439-1452.
[29] Tonino AJ, Therin M, Doyle C: Hydroxyapatite-coated femoral stems. Histology and histomorphometry around five components retrieved at post mortem. J Bone Joint Surg Br 1999; 81:148-154.
[30] Sennerby L, Ericson LE, Thomsen P, Lekholm U, Astrand P: Structure of the bone-titanium interface in retrieved clinical oral implants. Clin Oral Implants Res 1991; 2:103-111.
[31] Adell R, Lekholm U, Rockler B, Branemark PI: A 15-year study of osseointegrated implants in the treatment of the edentulous jaw. Int J Oral Surg 1981; 10:387-416.
[32] Albrektsson T, Wennerberg A: Oral implant surfaces: Part 1--review focusing on topographic and chemical properties of different surfaces and in vivo responses to them. Int J Prosthodont 2004; 17:536-543.
[33] Wennerberg A, Albrektsson T, Andersson B, Krol JJ: A histomorphometric and removal torque study of screw-shaped titanium implants with three different surface topographies. Clin Oral Implants Res 1995; 6:24-30.
[34] Wennerberg A, Hallgren C, Johansson C, Danelli S: A histomorphometric evaluation of screw-shaped implants each prepared with two surface roughnesses. Clin Oral Implants Res 1998; 9:11-19.
[35] Larsson C, Emanuelsson L, Thomsen P, Ericson LE, Aronsson BO, Kasemo B, Lausmaa J: Bone response to surface modified titanium implants - studies on the tissue response after 1 year to machined and electropolished implants with different oxide thicknesses. J Mater Sci Mater Med 1997; 8:721-729.
[36] Larsson C, Thomsen P, Aronsson BO, Rodahl M, Lausmaa J, Kasemo B, Ericson LE: Bone response to surface-modified titanium implants: studies on the early tissue response to machined and electropolished implants with different oxide thicknesses. Biomaterials 1996; 17:605-616.
[37] Larsson C, Thomsen P, Lausmaa J, Rodahl M, Kasemo B, Ericson LE: Bone response to surface modified titanium implants: studies on electropolished implants with different oxide thicknesses and morphology. Biomaterials 1994; 15:1062-1074.
[38] Al-Nawas B, Gotz H: Three-dimensional topographic and metrologic evaluation of dental implants by confocal laser scanning microscopy. Clin Implant Dent Relat Res 2003; 5:176-183.
[39] Gaggl A, Schultes G, Muller WD, Karcher H: Scanning electron microscopical analysis of laser-treated titanium implant surfaces--a comparative study. Biomaterials 2000; 21:1067-1073.
[40] Cho SA, Jung SK: A removal torque of the laser-treated titanium implants in rabbit tibia. Biomaterials 2003; 24:4859-4863.
[41] Brånemark R, Brånemark PI, Rydevik B, Myers RR: Osseointegration in skeletal reconstruction and rehabilitation: a review. J Rehabil Res Dev 2001; 38:175-181.
[42] Rydevik B: *Amputation prostheses and osseoperception in the lower and upper extremity*. In Brånemark P-I, Rydevik B, Skalak R, eds: Osseointegration in skeletal reconstruction and joint replacement. London: Guintessence Books, 1997, pp. 175–182.
[43] Hagberg K, Brånemark R, Gunterberg B, Rydevik B: Osseointegrated trans-femoral amputation prostheses: Prospective results of general and condition-specific quality of life in 18 patients at 2-year follow-up. Prosthet Orthot Int 2007; Accepted.
[44] Hagberg K, Haggstrom E, Uden M, Branemark R: Socket versus bone-anchored trans-femoral prostheses: hip range of motion and sitting comfort. Prosthet Orthot Int 2005; 29:153-163.
[45] Jacobs R, Branemark R, Olmarker K, Rydevik B, Van Steenberghe D, Branemark PI: Evaluation of the psychophysical detection threshold level for vibrotactile and pressure stimulation of prosthetic limbs using bone anchorage or soft tissue support. Prosthet Orthot Int 2000; 24:133-142.
[46] Ysander M, Branemark R, Olmarker K, Myers RR: Intramedullary osseointegration: development of a rodent model and study of histology and neuropeptide changes around titanium implants. J Rehabil Res Dev 2001; 38:183-190.
[47] Robinson K, Brånemark R, Ward D: *Future Developments: Osseointegration in Transfemoral Amputees*. In Smith D, Michael J, Bowker J, eds: Atlas of Amputations and Limb Deficiencies: Surgical, Prosthetic and Rehabilitation Principles, 2004, pp. 673-681.
[48] Wennerberg A, Albrektsson T, Ulrich H, Krol JJ: An optical three-dimensional technique for topographical descriptions of surgical implants. J Biomed Eng 1992; 14:412-418.
[49] Gadelmawla ES, Koura MM, Maksoud TMA, Elewa IM, Soliman HM: Roughness parameters. Journal of Materials Processing Technology 2002; 123:133-145.
[50] Wennerberg A: *On the surface roughness and implant incorporation*. Göteborg: Göteborg University, 1996, pp.
[51] Vösös J, Wieland M, Ruiz-Taylor L, Textor M, Brunette DM: *Characterization of Titanium Surfaces*. In Brunette DM, ed: Titanium in medicine : material science, surface science, engineering, biological responses and medical applications. Berlin: Springer, 2001, pp. 1019 s.
[52] Lausmaa J: Surface spectroscopic characterization of titanium implant materials. Journal of Electron Spectroscopy and Related Phenomena 1996; 81:343-361.
[53] Lausmaa J, Kasemo B: Surface spectroscopic characterization of titanium implant materials. Applied Surface Science 1990; 44:133-146.
[54] Cole DA, Shallenberger JR, Novak SW, Moore RL, Edgell MJ, Smith SP, Hitzman CJ, Kirchhoff JF, Principe E, Nieveen W, Huang FK, Biswas S, Bleiler RJ, Jones K: SiO2 thickness determination by x-ray

photoelectron spectroscopy, Auger electron spectroscopy, secondary ion mass spectrometry, Rutherford backscattering, transmission electron microscopy, and ellipsometry. Journal of Vacuum Science & Technology B: Microelectronics and Nanometer Structures 2000; 18:440-444.

[55] Conforto E, Caillard D, Aronsson BO, Descouts P: Crystallographic properties and mechanical behaviour of titanium hydride layers grown on titanium implants. Philosophical Magazine 2004; 84:631-645.

[56] Ask M, Rolander U, Lausmaa J, Kasemo B: Microstructure and Morphology of Surface Oxide-Films on Ti-6al-4v. J Mater Res 1990; 5:1662-1667.

[57] Radegran G, Lausmaa J, Mattsson L, Rolander U, Kasemo B: Preparation of ultra-thin oxide windows on titanium for TEM analysis. J Electron Microsc Tech 1991; 19:99-106.

[58] Lindsay MJ, Blackford MG, Attard DJ, Luca V, Skyllas-Kazacos M, Griffith CS: Anodic titania films as anode materials for lithium ion batteries. Electrochim Acta 2007; 52:6401-6411.

[59] Lewandowska M, Roguska A, Pisarek M, Polak B, Janik-Czachor M, Kurzydlowski KJ: Morphology and chemical characterization of Ti surfaces modified for biomedical applications. Biomol Eng 2007; 24:438-442.

[60] Sul YT, Johansson CB, Petronis S, Krozer A, Jeong Y, Wennerberg A, Albrektsson T: Characteristics of the surface oxides on turned and electrochemically oxidized pure titanium implants up to dielectric breakdown: the oxide thickness, micropore configurations, surface roughness, crystal structure and chemical composition. Biomaterials 2002; 23:491-501.

[61] Meredith N: Assessment of implant stability as a prognostic determinant. Int J Prosthodont 1998; 11:491-501.

[62] Meredith N, Book K, Friberg B, Jemt T, Sennerby L: Resonance frequency measurements of implant stability in vivo. A cross-sectional and longitudinal study of resonance frequency measurements on implants in the edentulous and partially dentate maxilla. Clin Oral Implants Res 1997; 8:226-233.

[63] Huang HM, Cheng KY, Chen CF, Ou KL, Li CT, Lee SY: Design of a stability-detecting device for dental implants. Proc Inst Mech Eng [H] 2005; 219:203-211.

[64] Franke Stenport V, Johansson CB: Evaluations of Bone Tissue Integration to Pure and Alloyed Titanium Implants. Clinical Implant Dentistry and Related Research 2008; Accepted for publication.

[65] Östman P-O: *On various protocols for direct loading of implant-supported fixed prostheses*. Göteborg: Department of Biomaterials, Institute of Clinical Sciences, Sahlgrenska Academy, Göteborg University, 2007, p. 102 s.

[66] Hollender L: *Radiographic Examination of Endosseous Implants in the Jaws*. In Worthington P, Brånemark P-I, eds: Advanced osseointegration surgery : applications in the maxillofacial region. Chicago: Quintessence, 1992, pp. 80-93.

[67] Stoppie N, van der Waerden JP, Jansen JA, Duyck J, Wevers M, Naert IE: Validation of microfocus computed tomography in the evaluation of bone implant specimens. Clin Implant Dent Relat Res 2005; 7:87-94.

[68] Morinaga K, Kido H, Sato A, Watazu A, Matsuura M: Chronological changes in the ultrastructure of titanium-bone interfaces: analysis by light microscopy, transmission electron microscopy, and micro-CT. Clinical Implant Dentistry and Related Research 2008; Accepted for publication.

[69] Brånemark R, Skalak R: An in-vivo method for biomechanical characterization of bone-anchored implants. Med Eng Phys 1998; 20:216-219.

[70] Donath K, Breuner G: A method for the study of undecalcified bones and teeth with attached soft tissues. The Sage-Schliff (sawing and grinding) technique. J Oral Pathol 1982; 11:318-326.

[71] Johansson CB, Morberg P: Importance of ground section thickness for reliable histomorphometrical results. Biomaterials 1995; 16:91-95.

[72] Johansson CB, Morberg P: Cutting directions of bone with biomaterials in situ does influence the outcome of histomorphometrical quantifications. Biomaterials 1995; 16:1037-1039.

[73] Hipp JA, Brunski JB, Cochran GV: Method for histological preparation of bone sections containing titanium implants. Stain Technol 1987; 62:247-252.

[74] Kihara A, Morimoto K, Suetsugu T: Improved method using a bubble-free adhesion technique for the preparation of semi-serial undecalcified histologic sections containing dental implants. J Oral Implantol 1989; 15:87-94.

[75] Pasyk KA, Hassett CA: Modified hematoxylin and eosin staining method for epoxy-embedded tissue sections. Pathol Res Pract 1989; 184:635-638.

[76] Albrektsson T, Brånemark PI, Hansson HA, Ivarsson B, Jönsson U: *Ultrastructural Analysis of the Interface Zone of Titanium and Gold Implants*. In Albrektsson T, Lee AJC, Brånemark PI, eds: Advances in biomaterials. Chichester: Wiley, 1982, pp. 167-177.

[77] Thomsen P, Ericson LE: Light and transmission electron microscopy used to study the tissue morphology close to implants. Biomaterials 1985; 6:421-424.

[78] Bjursten LM, Emanuelsson L, Ericson LE, Thomsen P, Lausmaa J, Mattsson L, Rolander U, Kasemo B: Method for ultrastructural studies of the intact tissue-metal interface. Biomaterials 1990; 11:596-601.

[79] Engqvist H, Botton GA, Couillard M, Mohammadi S, Malmstrom J, Emanuelsson L, Hermansson L, Phaneuf MW, Thomsen P: A novel tool for high-resolution transmission electron microscopy of intact interfaces between bone and metallic implants. J Biomed Mater Res A 2006; 78:20-24.

[80] Lausmaa J, Linder L: Surface spectroscopic characterization of titanium implants after separation from plastic-embedded tissue. Biomaterials 1988; 9:277-280.
[81] Murai K, Takeshita F, Ayukawa Y, Kiyoshima T, Suetsugu T, Tanaka T: Light and electron microscopic studies of bone-titanium interface in the tibiae of young and mature rats. J Biomed Mater Res 1996; 30:523-533.
[82] Steflik DE, Sisk AL, Parr GR, Hanes PJ, Lake F, Song MJ, Brewer P, McKinney RV: High-voltage electron microscopy and conventional transmission electron microscopy of the interface zone between bone and endosteal dental implants. J Biomed Mater Res 1992; 26:529-545.
[83] Futami T, Fujii N, Ohnishi H, Taguchi N, Kusakari H, Ohshima H, Maeda T: Tissue response to titanium implants in the rat maxilla: ultrastructural and histochemical observations of the bone-titanium interface. J Periodontol 2000; 71:287-298.
[84] Sennerby L, Thomsen P, Ericson LE: Ultrastructure of the bone-titanium interface in rabbits. Journal of Materials Science: Materials in Medicine 1992; 3:262-271.
[85] Brown SA, Simpson J: Electrochemical dissolution of metallic implants prior to histologic sectioning. J Biomed Mater Res 1979; 13:337-338.
[86] Rosengren A, Johansson BR, Danielsen N, Thomsen P, Ericson LE: Immunohistochemical studies on the distribution of albumin, fibrinogen, fibronectin, IgG and collagen around PTFE and titanium implants. Biomaterials 1996; 17:1779-1786.
[87] Rosengren A, Johansson BR, Thomsen P, Ericson LE: Method for immunolocalization of extracellular proteins in association with the implant-soft tissue interface. Biomaterials 1994; 15:17-24.
[88] Mohammadi S, Esposito M, Cucu M, Ericson LE, Thomsen P: Tissue response to hafnium. J Mater Sci Mater Med 2001; 12:603-611.
[89] Eriksson AS, Bjursten LM, Ericson LE, Thomsen P: Hollow implants in soft tissues allowing quantitative studies of cells and fluid at the implant interface. Biomaterials 1988; 9:86-90.
[90] Phaneuf MW: *FIB for materials science applications - a review*. In Giannuzzi LA, Stevie FA, eds: Introduction to Focused Ion Beams: Instrumentation, Theory, Techniques and Practice. Boston: Springer, 2005, pp.
[91] Young RJ, Moore MV: *Dual-Beam (FIB-SEM) System: Techniques and Automated Applications*. In Giannuzzi LA, Stevie FA, eds: Introduction to Focused Ion Beams: Instrumentation, Theory, Techniques and Practice. Boston: Springer, 2005, pp.
[92] Giannuzzi LA, Prenitzer BI, Kempshall BW: *Ion-solid interactions*. In Giannuzzi LA, Stevie FA, eds: Introduction to Focused Ion Beams: Instrumentation, Theory, Techniques and Practice. Boston: Springer, 2005, pp.
[93] Kaito T: *Three-Dimensional Nanofabrication Using Focused Ion Beams*. In Giannuzzi LA, Stevie FA, eds: Introduction to Focused Ion Beams: Instrumentation, Theory, Techniques and Practice. Boston: Springer, 2005, pp.
[94] Andersson R, Klepeis J: *Practical Aspects of FIB TEM Specimen Preparation*. In Giannuzzi LA, Stevie FA, eds: Introduction to Focused Ion Beams: Instrumentation, Theory, Techniques and Practice. Boston: Springer, 2005, pp.
[95] Langford RM, Petford-Long AK: Preparation of transmission electron microscopy cross-section specimens using focused ion beam milling. Journal of Vacuum Science & Technology a-an International Journal Devoted to Vacuum Surfaces and Films 2001; 19:2186-2193.
[96] Giannuzzi LA, Kempshall BW, Schwarz SM, Lomness JK, Prenitzer BI, Stevie FA: *FIB lift-out specimen preparation techniques: ex-situ and in-situ methods*. In Giannuzzi LA, Stevie FA, eds: Introduction to Focused Ion Beams: Instrumentation, Theory, Techniques and Practice. Boston: Springer, 2005, pp.
[97] Engqvist H, Schultz-Walz JE, Loof J, Botton GA, Mayer D, Phaneuf MW, Ahnfelt NO, Hermansson L: Chemical and biological integration of a mouldable bioactive ceramic material capable of forming apatite in vivo in teeth. Biomaterials 2004; 25:2781-2787.
[98] Hayashi Y, Yaguchi T, Ito K, Kamino T: High-resolution electron microscopy of human enamel sections prepared with focused ion beam system. Scanning 1998; 20:234-235.
[99] Hoshi K, Ejiri S, Probst W, Seybold V, Kamino T, Yaguchi T, Yamahira N, Ozawa H: Observation of human dentine by focused ion beam and energy-filtering transmission electron microscopy. J Microsc 2001; 201:44-49.
[100] Ngo H, Cairney J, Munroe P, Vargas M, Mount G: Focused ion beam in dental research. Am J Dent 2000; 13:31D-34D.
[101] Van Meerbeek B, Conn LJ, Jr., Duke ES, Schraub D, Ghafghaichi F: Demonstration of a focused ion-beam cross-sectioning technique for ultrastructural examination of resin-dentin interfaces. Dent Mater 1995; 11:87-92.
[102] Vilchis RJ, Hotta Y, Yamamoto K: Examination of enamel-adhesive interface with focused ion beam and scanning electron microscopy. Am J Orthod Dentofacial Orthop 2007; 131:646-650.
[103] Xie ZH, Mahoney EK, Kilpatrick NM, Swain MV, Hoffman M: On the structure-property relationship of sound and hypomineralized enamel. Acta Biomater 2007; 3:865-872.

[104] Engqvist H, Svahn F, Jarmar T, Detsch R, Mayr H, Thomsen P, Ziegler G: A novel method for producing electron transparent films of interfaces between cells and biomaterials. J Mater Sci Mater Med 2008; 19:467-470.
[105] Malmstrom J, Jarmar T, Adolfsson E, Engqvist H, Thomsen P: Structure of the interface between bone and scaffolds of zirconia and hydroxyapatite. In manuscript 2008.
[106] Giannuzzi LA, Giannuzzi NJ, Capuano MJ: FIB, SEM, and TEM of Bone/Dental Implant Interfaces. Microscopy and Microanalysis 2005; 11:998-999.
[107] Giannuzzi LA, Phifer D, Giannuzzi NJ, Capuano MJ: Two-dimensional and 3-dimensional analysis of bone/dental implant interfaces with the use of focused ion beam and electron microscopy. J Oral Maxillofac Surg 2007; 65:737-747.
[108] Goodhew PJ, Humphreys J, Beanland R: *Electron Microscopy and Analysis*. London and New York: Taylor and Francis, 2000, p. 264.
[109] Williams DB, Carter CB: *Transmission electron microscopy a textbook for materials science*. New York, N.Y.: Plenum Press, 1996, p. 729.
[110] Mohammadi S: *On the Tissue Response to Hafnium, Titanium and Thin Calcium Phosphate Coatings*. Department of Biomaterials. Göteborg: Göteborg University, 2003, pp. 89.
[111] Sul Y-T: *On the bone response to oxidized titanium implants : the role of microporous structure and chemical composition of the surface oxide in enhanced osseointegration*. Göteborg,, 2002, p. 94 s.
[112] Han CH, Johansson CB, Wennerberg A, Albrektsson T: Quantitative and qualitative investigations of surface enlarged titanium and titanium alloy implants. Clin Oral Implants Res 1998; 9:1-10.
[113] Johansson C, Lausmaa J, Röstlund T, Thomsen P: Commercially pure titanium and Ti6Al4V implants with and without nitrogen-ion implantation: surface characterization and quantitative studies in rabbit cortical bone. Journal of Materials Science: Materials in Medicine 1993; 4:132-141.
[114] Johansson CB, Han CH, Wennerberg A, Albrektsson T: A quantitative comparison of machined commercially pure titanium and titanium-aluminum-vanadium implants in rabbit bone. Int J Oral Maxillofac Implants 1998; 13:315-321.
[115] Johansson CB, Albrektsson T, Thomsen P, Sennerby L: Tissue reactions to titanium-6aluminum-4vanadium alloy. European Journal of Experimental Musculoskeletal Research 1992; 1:161-169.
[116] Sennerby L, Thomsen P, Ericson LE: Early tissue response to titanium implants inserted in rabbit cortical bone; Part II: Ultrastructural observations. Journal of Materials Science: Materials in Medicine 1993; 4:494-502.
[117] Meyer U, Joos U, Mythili J, Stamm T, Hohoff A, Fillies T, Stratmann U, Wiesmann HP: Ultrastructural characterization of the implant/bone interface of immediately loaded dental implants. Biomaterials 2004; 25:1959-1967.
[118] Listgarten MA, Buser D, Steinemann SG, Donath K, Lang NP, Weber HP: Light and transmission electron microscopy of the intact interfaces between non-submerged titanium-coated epoxy resin implants and bone or gingiva. J Dent Res 1992; 71:364-371.
[119] Steflik DE, Corpe RS, Lake FT, Sisk AL, Parr GR, Hanes PJ, Buttle K: Composite morphology of the bone and associated support-tissue interfaces to osseointegrated dental implants: TEM and HVEM analyses. Int J Oral Maxillofac Implants 1997; 12:443-453.
[120] Steflik DE, Corpe RS, Lake FT, Young TR, Sisk AL, Parr GR, Hanes PJ, Berkery DJ: Ultrastructural analyses of the attachment (bonding) zone between bone and implanted biomaterials. J Biomed Mater Res 1998; 39:611-620.
[121] Steflik DE, Corpe RS, Young TR, Sisk AL, Parr GR: The biologic tissue responses to uncoated and coated implanted biomaterials. Adv Dent Res 1999; 13:27-33.
[122] Steflik DE, Parr GR, Sisk AL, Hanes PJ, Lake FT: Electron microscopy of bone response to titanium cylindrical screw-type endosseous dental implants. Int J Oral Maxillofac Implants 1992; 7:497-507.
[123] Steflik DE, Sisk AL, Parr GR, Gardner LK, Hanes PJ, Lake FT, Berkery DJ, Brewer P: Osteogenesis at the dental implant interface: high-voltage electron microscopic and conventional transmission electron microscopic observations. J Biomed Mater Res 1993; 27:791-800.
[124] Steflik DE, Hanes PJ, Sisk AL, Parr GR, Song MJ, Lake FT, McKinney RV: Transmission electron microscopic and high voltage electron microscopic observations of the bone and osteocyte activity adjacent to unloaded dental implants placed in dogs. J Periodontol 1992; 63:443-452.
[125] Steflik DE, Parr GR, Sisk AL, Hanes PJ, Lake FT, Gardner LK, Berkery DJ: Morphology of the bone that supports endosteal dental implants. Transmission electron microscopic and high voltage electron microscopic observations. Oral Surg Oral Med Oral Pathol 1993; 76:467-475.
[126] Steflik DE, Parr GR, Sisk AL, Lake FT, Hanes PJ, Berkery DJ, Brewer P: Osteoblast activity at the dental implant-bone interface: transmission electron microscopic and high voltage electron microscopic observations. J Periodontol 1994; 65:404-413.
[127] Albrektsson T, Hansson HA: An ultrastructural characterization of the interface between bone and sputtered titanium or stainless steel surfaces. Biomaterials 1986; 7:201-205.
[128] Albrektsson T, Hansson HA, Ivarsson B: Interface analysis of titanium and zirconium bone implants. Biomaterials 1985; 6:97-101.

[129] Hansson HA, Albrektsson T, Branemark PI: Structural aspects of the interface between tissue and titanium implants. J Prosthet Dent 1983; 50:108-113.
[130] Johansson C, Lausmaa J, Ask M, Hansson HA, Albrektsson T: Ultrastructural differences of the interface zone between bone and Ti 6Al 4V or commercially pure titanium. J Biomed Eng 1989; 11:3-8.
[131] Linder L, Albrektsson T, Branemark PI, Hansson HA, Ivarsson B, Jonsson U, Lundstrom I: Electron microscopic analysis of the bone-titanium interface. Acta Orthop Scand 1983; 54:45-52.
[132] Thomsen P, Larsson C, Ericson LE, Sennerby L, Lausmaa J, Kasemo B: Structure of the interface between rabbit cortical bone and implants of gold, zirconium and titanium. J Mater Sci Mater Med 1997; 8:653-665.
[133] Okamatsu K, Kido H, Sato A, Watazu A, Matsuura M: Ultrastructure of the interface between titanium and surrounding tissue in rat tibiae--a comparison study on titanium-coated and -uncoated plastic implants. Clin Implant Dent Relat Res 2007; 9:100-111.
[134] Ayukawa Y, Takeshita F, Inoue T, Yoshinari M, Shimono M, Suetsugu T, Tanaka T: An immunoelectron microscopic localization of noncollagenous bone proteins (osteocalcin and osteopontin) at the bone-titanium interface of rat tibiae. J Biomed Mater Res 1998; 41:111-119.
[135] Ayukawa Y, Takeshita F, Yoshinari M, Inoue T, Ohtsuka Y, Shimono M, Suetsugu T, Tanaka T: An immunocytochemical study for lysosomal cathepsins B and D related to the intracellular degradation of titanium at the bone-titanium interface. J Periodontol 1998; 69:62-68.
[136] Linder L, Obrant K, Boivin G: Osseointegration of metallic implants. II. Transmission electron microscopy in the rabbit. Acta Orthop Scand 1989; 60:135-139.
[137] Porter AE, Botelho CM, Lopes MA, Santos JD, Best SM, Bonfield W: Ultrastructural comparison of dissolution and apatite precipitation on hydroxyapatite and silicon-substituted hydroxyapatite in vitro and in vivo. J Biomed Mater Res A 2004; 69:670-679.
[138] Porter AE, Buckland T, Hing K, Best SM, Bonfield W: The structure of the bond between bone and porous silicon-substituted hydroxyapatite bioceramic implants. J Biomed Mater Res A 2006; 78:25-33.
[139] Porter AE, Patel N, Skepper JN, Best SM, Bonfield W: Effect of sintered silicate-substituted hydroxyapatite on remodelling processes at the bone-implant interface. Biomaterials 2004; 25:3303-3314.
[140] Hench LL: Bioactive materials: the potential for tissue regeneration. J Biomed Mater Res 1998; 41:511-518.
[141] Brunette DM, Ratkay J, Chehroudi B: *Behaviour of Osteoblasts on Micromachined Surfaces*. In Davies JE, ed: The bone-biomaterial interface. Toronto: Univ. of Toronto Press, 1991, pp. 425-437.
[142] Ayukawa Y, Takeshita F, Inoue T, Yoshinari M, Ohtsuka Y, Murai K, Shimono M, Suetsugu T, Tanaka T: An Ultrastructural Study of the Bone-titanium Interface Using Pure Titanium-coated Plastic and Pure Titanium Rod Implants. Acta Histochem Cytochem 1996; 29:243-254.
[143] Linder L: High-resolution microscopy of the implant-tissue interface. Acta Orthop Scand 1985; 56:269-272.
[144] Serre CM, Boivin G, Obrant KJ, Linder L: Osseointegration of titanium implants in the tibia. Electron microscopy of biopsies from 4 patients. Acta Orthop Scand 1994; 65:323-327.
[145] Larsson C: *The interface between bone and metals with different surface properties: Light microscopic and ultrastructural studies*. Department of Biomaterials. Göteborg: Göteborg University, 1997, pp.
[146] Takeshita F, Ayukawa Y, Iyama S, Murai K, Suetsugu T: Long-term evaluation of bone-titanium interface in rat tibiae using light microscopy, transmission electron microscopy, and image processing. J Biomed Mater Res 1997; 37:235-242.
[147] Hemmerle J, Voegel JC: Ultrastructural aspects of the intact titanium implant-bone interface from undecalcified ultrathin sections. Biomaterials 1996; 17:1913-1920.
[148] Leize EM, Hemmerle J, Leize M: Characterization, at the bone crystal level, of the titanium-coating/bone interfacial zone. Clin Oral Implants Res 2000; 11:279-288.
[149] Albrektsson T, Jacobsson M: Bone-metal interface in osseointegration. J Prosthet Dent 1997; 57:597-607.
[150] Ericson LE, Johansson BR, Rosengren A, Sennerby L, Thomsen P: *Ultrastructural investigation and analysis of the interface of retrieved metal implants*. In Davies JE, ed: The bone-biomaterial interface. Toronto: Univ. of Toronto Press, 1991, pp. 425-437.
[151] Linder L: Ultrastructure of the bone-cement and the bone-metal interface. Clin Orthop Relat Res 1992:147-156.
[152] Albrektsson TO, Johansson CB, Sennerby L: Biological aspects of implant dentistry: osseointegration. Periodontol 2000 1994; 4:58-73.
[153] Heimann RB, Wirth R: Formation and transformation of amorphous calcium phosphates on titanium alloy surfaces during atmospheric plasma spraying and their subsequent in vitro performance. Biomaterials 2006; 27:823-831.
[154] Giannuzzi LA, Drown JL, Brown SR, Irwin RB, Stevie FA: Applications of the FIB lift-out technique for TEM specimen preparation. Microsc Res Tech 1998; 41:285-290.
[155] Giannuzzi LA, Stevie FA: A review of focused ion beam milling techniques for TEM specimen preparation. Micron 1999; 30:197-204.
[156] Sugiyama M, Sigesato G: A review of focused ion beam technology and its applications in transmission electron microscopy. J Electron Microsc (Tokyo) 2004; 53:527-536.
[157] Schwarz SW, Kempshall BW, Giannuzzi LA: Effects of diffusion induced recrystallization on volume diffusion in the Cu-Ni system. Acta Materialia 2003; 51:2765-2776.

[158] Abolhassani S, Gasser P: Preparation of TEM samples of metal-oxide interface by the focused ion beam technique. J Microsc 2006; 223:73-82.
[159] McCaffrey JP, Phaneuf MW, Madsen LD: Surface damage formation during ion-beam thinning of samples for transmission electron microscopy. Ultramicroscopy 2001; 87:97-104.
[160] Esposito M, Coulthard P, Thomsen P, Worthington HV: Interventions for replacing missing teeth: different types of dental implants. Cochrane Database Syst Rev 2005:CD003815.
[161] Esposito M, Coulthard P, Worthington HV, Jokstad A, Wennerberg A: Interventions for replacing missing teeth: different types of dental implants. Cochrane Database Syst Rev 2002:CD003815.
[162] Esposito M, Grusovin MG, Coulthard P, Thomsen P, Worthington HV: A 5-year follow-up comparative analysis of the efficacy of various osseointegrated dental implant systems: a systematic review of randomized controlled clinical trials. Int J Oral Maxillofac Implants 2005; 20:557-568.
[163] Esposito M, Murray-Curtis L, Grusovin MG, Coulthard P, Worthington HV: Interventions for replacing missing teeth: different types of dental implants. Cochrane Database Syst Rev 2007:CD003815.
[164] Esposito M, Worthington HV, Thomsen P, Coulthard P: Interventions for replacing missing teeth: different types of dental implants. Cochrane Database Syst Rev 2003:CD003815.
[165] Kasemo B, Lausmaa J: Biomaterial and implant surfaces: on the role of cleanliness, contamination, and preparation procedures. J Biomed Mater Res 1988; 22:145-158.
[166] Ask M, Lausmaa J, Kasemo B: Preparation and Surface Spectroscopic Characterization of Oxide-Films on Ti6a14v. Applied Surface Science 1989; 35:283-301.
[167] Kokubo T, Takadama H: How useful is SBF in predicting in vivo bone bioactivity? Biomaterials 2006; 27:2907-2915.
[168] Rossi S, Moritz N, Tirri T, Peltola T, Areva S, Jokinen M, Happonen RP, Narhi T: Comparison between sol-gel-derived anatase- and rutile-structured TiO2 coatings in soft-tissue environment. J Biomed Mater Res A 2007; 82:965-974.
[169] Moritz N, Areva S, Wolke J, Peltola T: TF-XRD examination of surface-reactive TiO2 coatings produced by heat treatment and CO2 laser treatment. Biomaterials 2005; 26:4460-4467.
[170] Moritz N, Jokinen M, Peltola T, Areva S, Yli-Urpo A: Local induction of calcium phosphate formation on TiO2 coatings on titanium via surface treatment with a CO2 laser. J Biomed Mater Res A 2003; 65:9-16.
[171] Lindberg F, Heinrich J, Ericsson F, Thomsen P, Engqvist H: Hydroxyapatite growth on single crystal rutil substrates. In manuscript 2008.
[172] Taborelli M, Jobin M, Francois P, Vaudaux P, Tonetti M, Szmukler-Moncler S, Simpson JP, Descouts P: Influence of surface treatments developed for oral implants on the physical and biological properties of titanium. (I) Surface characterization. Clin Oral Implants Res 1997; 8:208-216.
[173] Wieland M, Textor M, Chehroudi B, Brunette DM: Synergistic interaction of topographic features in the production of bone-like nodules on Ti surfaces by rat osteoblasts. Biomaterials 2005; 26:1119-1130.
[174] Ellingsen JE, Johansson CB, Wennerberg A, Holmen A: Improved retention and bone-tolmplant contact with fluoride-modified titanium implants. Int J Oral Maxillofac Implants 2004; 19:659-666.
[175] Hall J, Lausmaa J: Properties of a new porous oxide surface on titanium implants. Applied Osseointegration Research 2000; 1:5-8.
[176] Singh R, Kurella A, Dahotre NB: Laser surface modification of Ti--6Al--4V: wear and corrosion characterization in simulated biofluid. J Biomater Appl 2006; 21:49-73.
[177] Wennerberg A, Ektessabi A, Albrektsson T, Johansson C, Andersson B: A 1-year follow-up of implants of differing surface roughness placed in rabbit bone. Int J Oral Maxillofac Implants 1997; 12:486-494.
[178] Masaki C, Schneider GB, Zaharias R, Seabold D, Stanford C: Effects of implant surface microtopography on osteoblast gene expression. Clin Oral Implants Res 2005; 16:650-656.
[179] Buser D, Nydegger T, Oxland T, Cochran DL, Schenk RK, Hirt HP, Snetivy D, Nolte LP: Interface shear strength of titanium implants with a sandblasted and acid-etched surface: a biomechanical study in the maxilla of miniature pigs. J Biomed Mater Res 1999; 45:75-83.
[180] Zechner W, Tangl S, Furst G, Tepper G, Thams U, Mailath G, Watzek G: Osseous healing characteristics of three different implant types. Clin Oral Implants Res 2003; 14:150-157.
[181] Wennerberg A, Ohlsson R, Rosen BG, Andersson B: Characterizing three-dimensional topography of engineering and biomaterial surfaces by confocal laser scanning and stylus techniques. Med Eng Phys 1996; 18:548-556.
[182] Chen J, Mwenifumbo S, Langhammer C, McGovern JP, Li M, Beye A, Soboyejo WO: Cell/surface interactions and adhesion on Ti-6Al-4V: effects of surface texture. J Biomed Mater Res B Appl Biomater 2007; 82:360-373.
[183] Mwenifumbo S, Li M, Chen J, Beye A, Soboyejo W: Cell/surface interactions on laser micro-textured titanium-coated silicon surfaces. J Mater Sci Mater Med 2007; 18:9-23.
[184] Hall J, Miranda-Burgos P, Sennerby L: Stimulation of directed bone growth at oxidized titanium implants by macroscopic grooves: an in vivo study. Clin Implant Dent Relat Res 2005; 7 Suppl 1:S76-82.
[185] Bolind P, Acton C, Albrektsson T, Bonding P, Granstrom G, Johansson C, Lindeman P, Muhlbauer W, Tjellstrom A: Histologic evaluation of retrieved craniofacial implants. Otolaryngol Head Neck Surg 2000; 123:140-146.

[186] Bolind P, Johansson CB, Balshi TJ, Langer B, Albrektsson T: A study of 275 retrieved Branemark oral implants. Int J Periodontics Restorative Dent 2005; 25:425-437.
[187] Freese HL, Volas MG, Wood JR: *Metallurgy and Technological Properties of Titanium and Titanium Alloys*. In Brunette DM, ed: Titanium in medicine : material science, surface science, engineering, biological responses and medical applications. Berlin: Springer, 2001, pp. 1019 s.
[188] Guilherme AS, Henriques GE, Zavanelli RA, Mesquita MF: Surface roughness and fatigue performance of commercially pure titanium and Ti-6Al-4V alloy after different polishing protocols. J Prosthet Dent 2005; 93:378-385.
[189] Lin CW, Ju CP, Chern Lin JH: A comparison of the fatigue behavior of cast Ti-7.5Mo with c.p. titanium, Ti-6Al-4V and Ti-13Nb-13Zr alloys. Biomaterials 2005; 26:2899-2907.
[190] Carr AB, Larsen PE, Gerard DA: Histomorphometric comparison of implant anchorage for two types of dental implants after 3 and 6 months' healing in baboon jaws. J Prosthet Dent 2001; 85:276-280.
[191] Johansson CB, Albrektsson T, Ericson LE, Thomsen P: A quantitative comparison of the cell response to commercially pure titanium and Ti-6AI-4V implants in the abdominal wall of rats. Journal of Materials Science: Materials in Medicine 1992; 3:126-136.
[192] Wennerberg A, Ide-Ektessabi A, Hatkamata S, Sawase T, Johansson C, Albrektsson T, Martinelli A, Sodervall U, Odelius H: Titanium release from implants prepared with different surface roughness. Clin Oral Implants Res 2004; 15:505-512.
[193] Khan MA, Williams RL, Williams DF: The corrosion behaviour of Ti-6Al-4V, Ti-6Al-7Nb and Ti-13Nb-13Zr in protein solutions. Biomaterials 1999; 20:631-637.
[194] Khan MA, Williams RL, Williams DF: Conjoint corrosion and wear in titanium alloys. Biomaterials 1999; 20:765-772.
[195] Hallan G, Lie SA, Furnes O, Engesaeter LB, Vollset SE, Havelin LI: Medium- and long-term performance of 11,516 uncemented primary femoral stems from the Norwegian arthroplasty register. J Bone Joint Surg Br 2007; 89:1574-1580.
[196] Brånemark R, Thomsen P: Bone response to laser-induced micro- and nano-sized titanium surface features. In manuscript 2008.
[197] Palmquist A, Brånemark R, Thomsen P: *Bone response to laser-induced micro- and nano-sized titanium surface features*. 8th World Biomaterial Congress. Amsterdam, The Netherlands, 2008, pp.
[198] Esposito M, Coulthard P, Thomsen P, Worthington HV: The role of implant surface modifications, shape and material on the success of osseointegrated dental implants. A Cochrane systematic review. Eur J Prosthodont Restor Dent 2005; 13:15-31.
[199] Palmquist A, Jarmar T, Emanuelsson L, Taylor A, Taylor M, Engqvist H, Thomsen P: Calcium aluminate coated and un-coated free formed manufactured CoCr implants, a comparative study in rabbit. In manuscript 2008.
[200] Lawton DM, Oswald WB, McClure J: The biological reality of the interlacunar network in the embryonic, cartilaginous, skeleton: a thiazine dye/absolute ethanol/LR White resin protocol for visualizing the network with minimal tissue shrinkage. J Microsc 1995; 178:66-85.
[201] Davies JE: Bone bonding at natural and biomaterial surfaces. Biomaterials 2007; 28:5058-5067.